Research on Engineering Structures & Materials
www.jresm.org
Research Group

Research Article

ML driven optimization of mechanical properties in hybrid fiber-reinforced tertiary blended high-performance concrete

Mahesh[1,a], M.S. Shobha[1,b], Poornima Hulipalled[2,c], Veerabhadrappa Algur[*,3,d]

[1]*Department of Civil Engineering, Rao Bahadur Y Mahabaleswarappa Engineering College, Ballari, Visvesvaraya Technological University, Belagavi, Karnataka, India*
[2]*Department of Master of Computer Applications, Kishkinda University, Ballari, Karnataka, India*
[3]*Department of Mechanical Engineering, Rao Bahadur Y Mahabaleswarappa Engineering College, Ballari, Visvesvaraya Technological University, Belagavi, Karnataka, India*

Article Info

Article History:

Received 24 Aug 2024
Accepted 29 Nov 2024

Keywords:

Hybrid fiber concrete;
Combined tertiary mineral admixture;
Machine learning;
Structural construction

Abstract

This study focuses on optimizing the mechanical properties of hybrid fiber-reinforced tertiary blended high-performance concrete (HFRTHPC) by integrating CSF and polypropylene fibers (PPF) into a mix of silica fume (SF), metakaolin (MK), and fly ash (FA). These mineral admixtures replace Ordinary Portland Cement (OPC) at varying levels of 0%, 15%, 22.5%, and 30%. A comprehensive analysis was conducted on 80 different concrete mixes, each with W/B ratios ranging from 0.275 to 0.375, and a total fiber content of 1.25% (0.5%-1% CSF and 0.25% PPF). The results showed a significant increase in compressive strength, with a maximum improvement of 30.24% after 28 days of curing. The optimal mix was identified as containing 5% SF, 5% MK, 5% FA, 1% CSF, and 0.25% PPF at a W/B ratio of 0.275. Additionally, regression equations were developed to predict the mechanical properties. The study also utilized three machine learning techniques—AdaBoost Regressor, Random Forest, and Extreme Gradient Boost Regressor—to model compressive, split tensile, and flexural strengths. Among these, the Extreme Gradient Boost Regressor exhibited superior predictive accuracy and generalization capabilities. This research offers valuable insights for optimizing sustainable concrete compositions and provides a foundation for future advancements in concrete technology.

1. Introduction

In contrast to normal concrete, high-performance concrete (HPC) is developed with superior characteristics such as enhanced strength, durability, workability, and improved resistance to environmental factors. These qualities are achieved by incorporating low water-to-cement ratios and high-quality pozzolanic materials such as FA, SF, ground granulated blast furnace slag (GGBS), MK, and superplasticizers. High-performance concrete can involve up to 10 ingredients, focusing on strength and durability. The partial replacement of cement with one, two, or three pozzolanic materials can be termed binary, ternary, and tertiary/quaternary concrete mixes, respectively. Tertiary systems combining the pozzolanic materials offer advantages, blending silica fume and metakaolin with fly ash improves early strength, while fly ash enhances workability. This synergy is crucial for HPC development. Tertiary mixtures, including fly ash/GGBS, silica fume, and metakaolin, provide high strength, low permeability, corrosion and sulfate resistance, ASR resistance, and reduced thermal cracking. HPC represents a specialized form of concrete

*Corresponding author: veereshalgur@gmail.com
[a]orcid.org/0009-0009-8110-7267; [b]orcid.org/0009-0001-1059-9606; [c]orcid.org/0000-0003-4680-8120; [d]orcid.org/0000-0001-6094-6197
DOI: http://dx.doi.org/10.17515/resm2024.409me0829rs

engineered for specific applications and environmental conditions, ensuring optimal performance over the structure's design lifespan and exposure to varying loads and environments [1]. The blended concretes use fly ash, silica fume, ground granulated blast furnace slag, and metakaolin as partial cement replacements. These admixtures lower cement content, reducing the environmental impact of cement production. Reviewed research articles highlight improvements in mechanical properties, durability, workability, enhanced thermal performance, and long-term strength. The use of industrial by-products and potential cost savings are also noted [2]. In quaternary binders made with GGBS, FA, MK, and SF as partial replacements for Ordinary Portland Cement (OPC), the study focused on standard consistency, initial and final setting time. SF significantly increases water requirements due to its high surface area, while GGBS reduces the water/binder ratio. SF and GGBS extend setting time at various replacement levels, whereas SF and MK initially increase setting time but decrease at higher replacements. On the whole, the admixtures in the quaternary binder mix impact independently, with SF and MK notably enhancing consistency [3]. The effects of incorporating mineral admixtures such as FA, SF, GGBS, MK, and rice husk ash (RHA) on the properties of fresh concrete have been reviewed. The study compares normal and high-strength concrete partially replaced with these admixtures. The admixtures are classified into two types: chemically active (decreased workability and setting time but increased heat of hydration and reactivity) and micro fillers (increased workability and setting time but reduced heat of hydration and reactivity). While the small particle size and higher specific surface area of these admixtures improve concrete density and impermeability, they also lower workability, necessitating the use of superplasticizers [4]. Fly ash concrete typically had lower compressive strength. In contrast, binary combinations of Portland cement with silica fume or slag, as well as ternary combinations including both slag and silica fume, exhibited significantly higher compressive strengths. The addition of mineral admixtures also resulted in reduced water permeability values [5]. The quaternary binders with 50% partial replacement of OPC and 30% FA with 10% M/GGBS showed the highest compressive strength with a low water/binder ratio. An enhancement of about 25% and 10% higher flexural strength and around 11.9% and 11.2% in split tensile strength at longer ages were noted [6]. Enhanced compressive, split tensile and flexural strength was noticed for a quaternary blend of cement with 20% fly ash, 10% Lime powder, and 10% rice husk ash, for this same blend the corrosion resistance also levelled up [7]. Incorporating pozzolanic materials enhances concrete's resistance to aggressive agents, such as sulfuric acid. These additions reduce the amount of calcium hydroxide, which is most susceptible to acid attacks [8]. Concrete is brittle and weak in tension; early concrete hardening is prone to microcracks caused by environmental and load fluctuations. These limitations lead to the development of fiber-reinforced concrete (FRC). Initial studies on FRC focused on using single fiber types, demonstrating enhanced concrete properties, particularly in strength and durability, as fibers prevent surface cracking and improve impact strength. Current research has driven interest toward fiber hybridization, combining metallic and non-metallic fibers to leverage their respective advantages. Steel fibers enhance tensile strength, toughness, and stiffness, while fibers like PPF contribute to elasticity, mixability, and resistance. Combining these fibers results in composite fiber-reinforced concrete exhibiting superior strength properties compared to individual fibers [9-13]. Studies suggest that reinforced concrete containing 0.3% PPF demonstrates superior flexural and compressive strength compared to content levels up to 0.5%. The research reveals that the mix design with 0.3% PPF achieved the highest strength, with minimal variance (1.0% - 3.0%) from mixes with 0.25% PPF. As a result, 0.25% PPF was chosen for the experiment [14-15]. In examining CSF mechanical properties with an aspect ratio of 50, the research revealed that 3.0% CSF blends outperformed mixes with 0% to 2.0% fibers. Among all aspect ratios studied, CSF with an aspect ratio of 50 showed statistically better results in terms of strength. The study concluded that adding CSF up to 1% improved HPC strength meanwhile higher levels led to decreased compressive and tensile strengths, accompanied by drawbacks such as diminished ductility, increased cost, and reduced workability. CSF's primary role is crack prevention [16-17]. Research on enhancing structural strength and seismic resistance through fiber integration in concrete found that a composite blend of 80% crimped steel fiber and 20% polyolefin fiber showed robust qualities [18]. With the incorporation of CSF at levels of 0.55, 1.0% and 1.5%, HPC exhibited enhanced impact strength. The initiation strength for the first failure crack rose to 139%, 268%, and 366% and to 129%, 238%, and 321%, respectively, compared to

normal concrete [19-20]. For a combined mix of cement, 20% GGBS, 10% MK, steel and glass fiber at 2% showed an increase in compressive and split strength for a grade of M60 [21-22]. Optimal results were observed by replacing 10.0% of the cement with Metakaolin (MK), leading to increased compression strength at rates of 7%, 16.75%, 11.42%, and 6.0% for partial cement replacements of 5%, 10%, 15%, and 20% with MK, respectively [23]. The study highlights the importance of understanding the effective utilization of mineral admixtures in mortar. The findings are significant for optimizing the use of mineral admixtures in engineering applications, ensuring that they contribute to the desired properties of the mortar without remaining unreacted. Under a curing temperature of 30°C, when the replacement ratio exceeded 30%, the change in $Ca(OH)_2$ amount with replacement ratio was nearly linear. At this point, the excess fly ash essentially stopped consuming $Ca(OH)_2$. [24]. This study explored the strength and durability of HFRHPC with SF as an admixture. Using fixed PF and varying CF, it achieved significant gains in compressive (35.18%), split tensile (40.35%), and flexural strengths (71.54%) at 28 days [25]. This study examined HFRHPC incorporating FA as an admixture, with polypropylene and varying crimped steel fibers. Testing different FA levels and water-to-binder ratios, results revealed 1.25% hybrid fibers with 10% FA provided optimal strength, durability, and acid resistance, sustaining performance for 90 days [26]. This study assessed the effects of MK and hybrid fibers on High-Performance Concrete. With 0.25% polypropylene and varying steel fibers, results showed significant strength gains. Optimal mix—1.25% hybrid fibers with 10% MK—achieved peak compressive (37.05%), split tensile (42%), flexural (74.41%), and impact (68.32%) strengths after 28 days [27]. This study investigated the effects of combining Fly Ash, Silica Fume, Glass Fibers, and Polypropylene Fibers in Composite-Fiber Reinforced High-Performance Concrete. The optimal mix—5% FA and SF, with 1% GF and 0.25% PPF at a 0.275 W/B ratio—achieved maximum strength [28].

The ANOVA analysis revealed that different substitution levels of all three components significantly impacted the fresh and hardened properties of SCLCs. The findings showed that adding CS or MS to SCLC specimens improved the previously mentioned parameters, while ternary mixes with both MS and CS delivered the best performance [29]. The application of machine learning (ML) techniques, which make a significant contribution to the field of civil engineering by accurately predicting the mechanical properties of concrete, is particularly important. In recent times, the growth of soft-computing methodologies has given rise to ML as a reliable and accurate instrument for computer modeling. ML has become widely acknowledged as an effective methodology that can be implemented across diverse research domains, including concrete structures [30-31]. Studies have employed ML methods. During the training phase, the R-square value of the deep learning models was roughly 0.960, and during the testing phase, it was slightly above 0.940. But when it came to performance, the GRU model outperformed the others, as evidenced by an R-square value that was extremely greater than 0.990 in the learning phase and close to 0.961 in the testing phase. These findings point to the GRU model's excellent efficacy and accuracy in both phases [32]. The findings of the investigation showed that the suggested equations performed better at properly predicting than traditional techniques such as the linear regression model (LRM). In contrast to the LRM, the suggested equations produced lower values for MAE and RMSE and showed a higher coefficient of determination (R2) [33]. Compared to conventional approaches, ML provides better predictions for required mechanical characteristics [34-35]. Several studies have employed ML methods to predict the strength properties of conventional concrete [36-39]. ML methods are employed to forecast concrete strength [40-57] and the durability of concrete [58-59]. Nevertheless, the use of ML methods to predict compressive, flexural, and splitting tensile strengths in fiber-reinforced concrete is still not widely explored.

While extensive research has examined binary and ternary pozzolanic material combinations, limited studies explore the complex interactions and optimal mix proportions in tertiary/quaternary blends. More research is needed on the synergistic effects of materials like fly ash, silica fume, GGBS, and metakaolin across various proportions and environmental conditions. Regarding fiber optimization and hybridization in high-performance concrete (HPC), studies have shown enhanced properties with hybrid fibers, such as steel and polypropylene. However, the ideal fiber types, contents, and ratios for maximizing performance metrics like compressive strength,

splitting tensile strength, flexural strength, and impact resistance are still underexplored, especially in HPC applications. Further research is also required on the long-term effects of fiber hybridization in HPC.

Machine learning (ML) has been applied to predict mechanical properties in both conventional and HPC, yet its application to fiber-reinforced high-performance concrete (FR-HPC) is limited. There is a clear research gap in using ML techniques to accurately predict FR-HPC's compressive, flexural, and splitting tensile strengths. Additionally, achieving meaningful results with ML will require substantial input data collection. In order to get the desired findings, ML methods require the collection of an input dataset. To achieve this objective, we utilized eight input parameters, including W/B, cement, metakaolin, silica, fly ash, crimped steel fibers, polypropylene fibers, and the age of the specimens. The experiments were conducted using an absolute volume methodology for concrete mix design, while data points comprising the results of the experiments were gathered for algorithm implementation.

2. Experimental Program

2.1 Materials Used

In the current experimental study, OPC grade 43 as per IS 8112:1989, along with mineral admixtures such as FA, SF, and MK, were utilized. The physical and chemical properties of these materials are detailed in Tables 1. Local river sand served as the fine aggregate, while the crushed stone as coarse aggregate was also sourcing from local. Fine and Course aggregate physical properties provided in Table 2. To produce the concrete mix, the superplasticizer SP-430 was employed. Additionally, CSF and PPF were incorporated into the experiment, with their characteristics listed in Table 3.

Table 1. Physical and chemical properties of cement and mineral admixtures

Physical Properties	Cement	Fly ash	Metakaolin	Silica fume
Specific gravity.	3.12	2.17	2.61	2.21
Mean grain siz(μm)	8 -210	20-25	2.53	1.14
Specific area (cm^2/g)	2947	3988	15,000 to18,000	18,000 to30,000
Color	Grey.	Tan to dark grey.	Ivory to cream.	light to darkgrey.
Chemical Properties	Fly Ash (FA)	Metakaolin (MK)	Silica Fume (SF)	Code IS 3812 Requirement
Silica (SiO_2)	59.16	60-65	92.3	(SiO_2)+
Aluminum (Al_2O_3)	30.64	43.18	1.3	(Al_2O_3)+
Iron oxide (Fe_2O_3)	4.70	0.6	1.0	(Fe_2O_3) = 70.0 (min)
Calcium oxide (CaO)	2.85	1.06	1.6	--
Magnesium oxide(MgO)	0.36	0.61	0.9	5.0 (Max)
Loss on ignition	0.21	0.70	1.53	6.0(Max)

Table 2. Physical properties Fine and Coarse aggregate

Properties	fine aggregate	coarse aggregate
Specific gravity	2.68	2.75
Fineness modulus	2.74	6.73
Bulk density		
i) Loose	14.67 kN/m^3	13.291 kN/m^3
ii) Compacted	16.04 kN/m^3	15.001 kN/m^3
Grading	Zone – II	--

Table 3. Physical properties fibers

Properties	CSF	PPF
Specific Gravity	7.85	0.912
Tensile strength (MPa)	1050	530
Density (kg/m^3)	7850	910
Length of fiber (mm)	30	12
Equivalent diameter (mm)	0.60	0.35
Shape	crimped	monofilament

Fig. 1. Crimped steel fibers

Fig. 2. Polypropylene fibers

Fig. 3. The materials employed in the current study include

2.2 Materials and Mix Proportioning

In this experiment, mix proportions were assessed using an absolute volume approach. Ingredients were measured by volume and then converted to weight to ensure a uniform mixture. All ingredients were dry-mixed initially, with steel and polypropylene fibers added in this phase. Water and a superplasticizer were then introduced to achieve a homogeneous concrete mix. Table.4 provides the percentage dosage of each component in the sample. Mix identification employed a coding system: the first three Alphabets CTM represents combined tertiary mineral admixture, MK, SF, and FA. The subsequent number indicated the collective percentage of cement replaced by combining MK, SF, and FA. Alphabets P, Q, R, and S represented composite fiber matrices with varying CSF and PPF percentages: P (0% CSF +0% PPF), Q (0.50% CSF + 0.25% PPF), R (0.75% CSF + 0.25% PPF), and S (1.0% CSF + 0.25% PPF). The final letter indicated the A/B ratio (A = 1.75), the W/B ratios were depicted by the last number (1= 0.275, 2 = 0.300, 3 =

0.333, 4 = 0.350, and 5 = 0.375). For instance, a reference mix with A/B = 1.75 and W/Bof 0.275 and 788.29 kg/m^2 of cement was denoted as CTM0PA1, signifying the absence of fibers and mineral admixtures. Another mix, CTM15PA1 used 660.37 kg/m^2 of cement and 38.85 kg/m^2 of each MK, SF, and FA, indicating a specific combination of fibers and mineral admixtures. The nomenclature and compositions of various mixes are detailed in Table 4, maintaining consistent design principles across different W/B ratios to ensure a comprehensive assessment.

Table. 4 Mix. proportions of HFRHPTC mix for W/B= 0.275.

Mix designation	Cement (%)	MK (%)	SF (%)	FA (%)	CSF (%)	PPF (%)	Total percentage of tertiary mineral composition
CTM0PA1	100	0	0	0	0	0	0
CTM15PA1	85	5	5	5	0	0	15
CTM22.5PA1	77.50	7.50	7.50	7.50	0	0	22.5
CTM30PA1	70	10	10	10	0	0	30
CTM0QA1	100	0	0	0	0.50	0.25	0
CTM15QA1	85	5	5	5	0.50	0.25	15
CTM22.5QA1	77.50	7.50	7.50	7.50	0.50	0.25	22.5
CTM30QA1	70	10	10	10	0.50	0.25	30
CTM0RA1	100	0	0	0	0.75	0.25	0
CTM15RA1	85	5	5	5	0.75	0.25	15
CTM22.5RA1	77.50	7.50	7.50	7.50	0.75	0.25	22.5
CTM30RA1	70	10	10	10	0.75	0.25	30
CTM0SA1	100	0	0	0	1.00	0.25	0
CTM15SA1	85	5	5	5	1.00	0.25	15
CTM22.5SA1	77.50	7.50	7.50	7.50	1.00	0.25	22.5
CTM30SA1	70	10	10	10	1.00	0.25	30

*Similarly designs of constituents are used for other W/B ratios W/B= 0.300(2), 0.325(3), 0.350(4), and 0.375(5)

2.3 Experimental Methods

The compressive strength of concrete-cubic specimens (100 x 100 x 100 mm) was tested as per ASTM C39. The split tensile strength of concrete-cylinder specimens (150 mm diameter, 300 mm height) was evaluated following ASTM C496, and the flexural strength of concrete-prism or beam specimens (500 x 100 x 100 mm) was tested in accordance with ASTM C78. After demolding, all specimens were cured for 28 days. Cubic and cylindrical specimens were tested using a digital compression testing machine as per IS 14858, while prism or beam specimens were tested using a universal testing machine as per IS 516-1959. Each test was conducted with three samples per combination, and the average values are reported.

2.4 Machine Learning Approach

Within the scope of this investigation, the experiment yielded a total of 320 data samples and was utilized for the purpose of training ML methods. During data collection, the proportions of the combination and the output that was intended were taken into consideration. This was carried out to satisfy the requirements because the models needed the same input variables for every mixture to reliably estimate the outcomes.

The distribution of data trials used in testing and training the model was 30% and 70%, respectively. The levelof accuracy of a model can be assessed by examining the R^2 result of the projected outcome. Values closer to zero indicate a greater degree of variance, while values that are closer to one show a close alignment between the prediction model and experimental data. The statistical measures, including mean absolute error (MAE), mean square error (MSE), and root mean squared error (RMSE), were employed to measure the exactness of a model. Further details about the machine learning (ML) models and optimization techniques used in this investigation are covered in the sections that follow.

2.4.1 Ensemble Machine learning

In contrast to conventional machine learning, which typically employs a single model, ensemble learning makes use of multiple models. Ensemble methods construct a final prediction by combining the predictions of multiple models, as opposed to relying on the estimates of a single model. It results in enhanced efficacy in comparisonto standalone models. Through the utilization of three ensemble methods, namely Ada Boost (AdaB), random forest (RF), and extreme gradient boost (XGB), they have the capacity to significantly diminish errors, enhance precision, and augment generalizability. The important tuning parameters of the three ML models are listed in Table 5 to produce better performance.

2.4.2 Ada Boost

The AdaB regressor approach starts by training a weak learner on the original dataset with identical weights for each data point. In future rounds, it concentrates on misclassified occurrences, modifying the weights to emphasize difficult cases. It distributes weights to each weak learner based on their performance, and their predictions are combined in a weighted sum to get the final prediction. The mentioned iterative approach persists until the desired number of weak learners has been reached [52]. AdaB's adaptability to complicated datasets and ability to reduce overfitting make it an effective tool for regression tasks. In Python, the scikit-learn library includes the AdaBoost Regressor class for the implementation, which commonly uses decision trees as weak learners. AdaBoost Regressor stands out for its ensemble method, which provides robustness and increased generalization across a variety of regression settings. The final prediction for a new input X is the weighted sum of weak learner predictions:

$$\hat{y}(X) = \sum_{t=1}^{T} \alpha_t h_t(X) \tag{1}$$

Where; $\hat{y}(X)$ is anticipated output for input X, T represents the total count of weak learners, α_t is the weight assigned to the t-th weak learner, $h(X)$ is the prediction of the t-th weak learner for input X. AdaB creates a resilient and accurate ensemble model for regression tasks by combining weak learners thatfocus on different parts of the data.

2.4.3 Random Forest

RF is an ensemble learning approach for regression tasks that combines predictions from various decision trees to increase accuracy and decrease overfitting. In this model, decision trees serve as base learners, and the algorithm incorporates randomization by taking only a subset of characteristics at each split and using bootstrapped sampling [50]. The training procedure entails creating numerous trees independently, and during prediction, the final output is frequently an average of individual tree forecasts. This method improves resilience and handles non-linear connections effectively. RF provides insights regarding feature relevance, which helps with feature selection. In Python, the scikit-learn library provides the Random Forest Regressor class for easy implementation. For a given input X, the RF prediction is the mean of predictions from all the individual trees:

$$\hat{y}(X) = \frac{1}{N} \sum_{t=1}^{N} T_t(X) \tag{2}$$

Where; $\hat{y}(X)$ is the predicted output for input X, N is number of trees, (X) is prediction of the t-th tree for input X.

2.4.4 XG Boost

XGB Regressor, a gradient-boosting extension, is efficient, scalable, and regularized for regression applications.For better prediction, the system creates decision trees sequentially, correcting earlier errors. To avoid overfitting, the function minimizes the difference between the expected and actual values while penalizingmodel complexity using a regularization factor. The final forecast is the sum of all tree predictions. Regularization terms control tree complexity in XGB, improving

generalization to fresh data [54]. XGBoost efficiently handles massive datasets and uses feature-important insights to choose features. The number of trees, learning rate, tree depth, and minimum child weight must be tuned. The XGB Regressor class from the XGBoost package in Python is used for implementation. XGB is used for varied regression scenarios that require accurate and robust predictions due to its versatility. The XGB minimizes an objective function that combines a loss function measuring the difference between the actual and anticipated values with a regularization term. The function for XGB is defined as follows:

$$Objective = \sum_{i=1}^{n} L(y_i, \hat{y}_i) + \sum_{k=1}^{K} \Omega(f_k) \quad (3)$$

Where; n is the number of samples used for training, y_i is the actual value for the i-th sample, $\hat{y}_i$ is the predicted value for the i-th sample, $L(y_i, \hat{y}_i)$ is the loss function measuring the difference between the true and predicted values, K represents leaves in the tree, f_k is the score associated with the k-th leaf, $\Omega(f_k)$ is the regularization.

The regularization term and loss function are parameter and hyperparameter sensitive. Mean Squared Error andAbsolute Loss are two popular loss functions used in regression applications.

2.4.5 Validation of models

Evaluation metrics quantify a machine learning model's performance on a regression task. They help to assess model prediction accuracy and impact model selection and optimization. Evaluation metrics provide quantitativeperformance data to the machine learning pipeline, assisting in the creation, optimization, and deployment of models. The ML algorithms were verified using statistical error assessments like MAE, MSE, RMSE, and R^2 onthe test dataset and the k-fold approach while training the models. In this study, we have used 10-fold validations. The k-fold technique utilizes multiple train-test splits and averages the results to reduce the variancein the performance estimate and provide a more robust assessment of the model's effectiveness.

$$MAE = \frac{1}{N}\sum_{i=1}^{n} |F_i - V_i| \quad (4)$$

$$MSE = \frac{1}{N}\sum_{i=1}^{n} (F_i - V_i)^2 \quad (5)$$

$$RMSE = \sqrt{MSE} \quad (6)$$

$$R^2 = 1 - \frac{\sum_{n=1}^{n}(V_i - F_i)^2}{(V_i - V)^2} \quad (7)$$

Where n = number of data points, V_i F_i = predicted findings, and V_i = actual results, V = mean of actual values

3. Results and Discussion

3.1 Experimental Approach

3.1.1 Compression Strength

The cube compressive strength at 7 and 28 days cuing of combined tertiary mineral admixture-based HFRHPTC concrete mix results are presented in Table 6.

Table 6. Cube compressive strength of Tertiary mineral admixture based HPC mix

Mix Designation	Cube compressive strength MPa		Mix Designation	Cube compressive strength MPa	
	7 days	28 days		7 days	28 days
CTM0PA1	59.04	73.9	CTM0RA3	59.34	75.17
CTM15PA1	67.99	85.18	CTM15RA3	70.03	88.23

CTM22.5PA1	62.99	78.57	CTM22.5RA3	63.64	78.44
CTM30PA1	57.85	71.93	CTM30RA3	57.31	71.72
CTM0QA1	60.84	75.84	CTM0SA3	61.24	76.34
CTM15QA1	72.55	91.55	CTM15SA3	72.23	90.32
CTM22.5QA1	65.24	81.83	CTM22.5SA3	65.42	80.72
CTM30QA1	59.69	74.29	CTM30SA3	59.06	73.08
CTM0RA1	62.56	79.68	CTM0PA4	53.29	68.63
CTM15RA1	74.99	93.47	CTM15PA4	60.72	78.42
CTM22.5RA1	67.94	83.34	CTM22.5PA4	55.99	71.39
CTM30RA1	61.2	76	CTM30PA4	52.71	66.71
CTM0SA1	64.5	80.1	CTM0QA4	55.03	70.33
CTM15SA1	76.89	95.69	CTM15QA4	64.28	83.58
CTM22.5SA1	70.15	85.55	CTM22.5QA4	57.42	75.29
CTM30SA1	63.09	76.29	CTM30QA4	53.98	68.13
CTM0PA2	57.09	72.39	CTM0RA4	57.2	73.44
CTM15PA2	65.1	83.04	CTM15RA4	66.3	86.3
CTM22.5PA2	60.79	76.54	CTM22.5RA4	61.04	77.04
CTM30PA2	55.66	69.99	CTM30RA4	56.21	70.41
CTM0QA2	58.77	73.63	CTM0SA4	58.03	75.37
CTM15QA2	69.9	88.93	CTM15SA4	68.16	88.72
CTM22.5QA2	62.98	79.28	CTM22.5SA4	62.25	78.39
CTM30QA2	57.22	72.08	CTM30SA4	57.22	72.04
CTM0RA2	61.14	75.6	CTM0PA5	52.72	66.98
CTM15RA2	72.22	91.03	CTM15PA5	60.24	76.04
CTM22.5RA2	65.55	81.15	CTM22.5PA5	53.43	69.43
CTM30RA2	59.02	74.02	CTM30PA5	50.75	64.75
CTM0SA2	62.53	78.42	CTM0QA5	54.34	68.24
CTM15SA2	73.88	93.2	CTM15QA5	63.53	81.13
CTM22.5SA2	67.62	83.59	CTM22.5QA5	55.57	73.02
CTM30SA2	60.92	75.01	CTM30QA5	52.18	66.93
CTM0PA3	55.6	70.82	CTM0RA5	55.66	72.56
CTMF15PA3	63.28	81.47	CTM15RA5	65.28	84.08
CTM22.5PA3	58.86	74.16	CTM22.5RA5	57.09	75.19
CTM30PA3	53.98	67.88	CTM30RA5	52.96	68.66
CTM0QA3	57.33	71.37	CTM0SA5	57.46	73.12
CTM15QA3	67.25	86.15	CTM15SA5	67.01	86.54
CTM22.5QA3	61.11	76.87	CTM22.5SA5	59.12	77.05
CTM30QA3	55.47	70.07	CTM30SA5	55.19	69.29

3.1.1.1 Effect of Water-Binder Ratio on Cube Compressive Strength Of Tertiary Mineral Admixture Based HPC Mix With Hybrid-Fibers

The variation of cube compressive strength for blended tertiary mineral admixture-based HPC mix with different W/B ratios is shown in Figures 4 and 5, with results detailed in Table 6 for 7-day and 28-day compressive strength. It can be observed that the compressive strength of HFRHPTC mix declines as the W/B ratio increases from 0.275 to 0.375, which is similar to the behavior of plain HPC mix. The highest compressive strength of HFRHPTC mix at both 7 and 28 days for all W/B ratios is observed with 15% cement replaced by blended tertiary mineral admixture. The maximum cube compressive strength attained at 7 days is 76.88 MPa for the CTM15SA1 mix with a W/B ratio of 0.275. For the same mix, with W/B ratios ranging from 0.300 to 0.375, the strength was reduced by 6.07% to 15.10%, respectively. Similar trends are observed for the 28-day compressive strength, which was 95.68 MPa for the CTM15SA1 mix with a W/B ratio of 0.275. For the same mix, with W/B ratios ranging from 0.300 to 0.375, the strength was reduced by 4.87% to 12.13%, respectively.

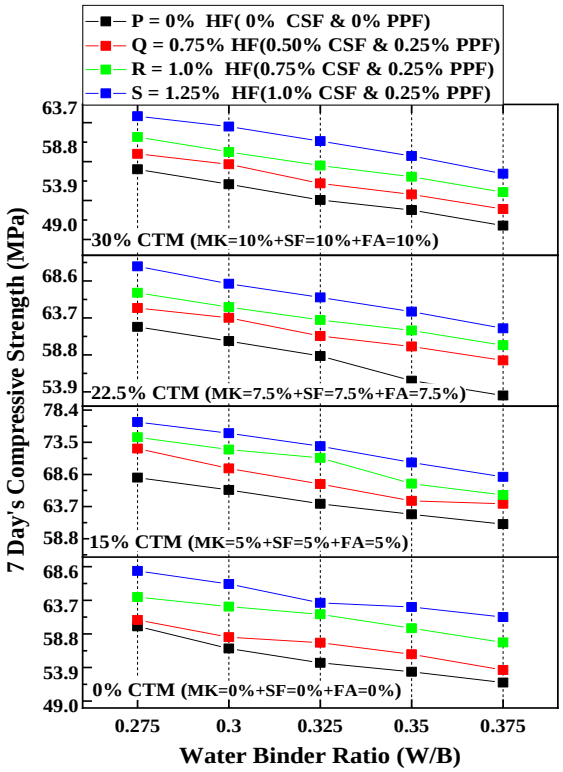

Fig. 4. Seven days Cube compression strength Vs. W/B ratio for HFRTHPC mix

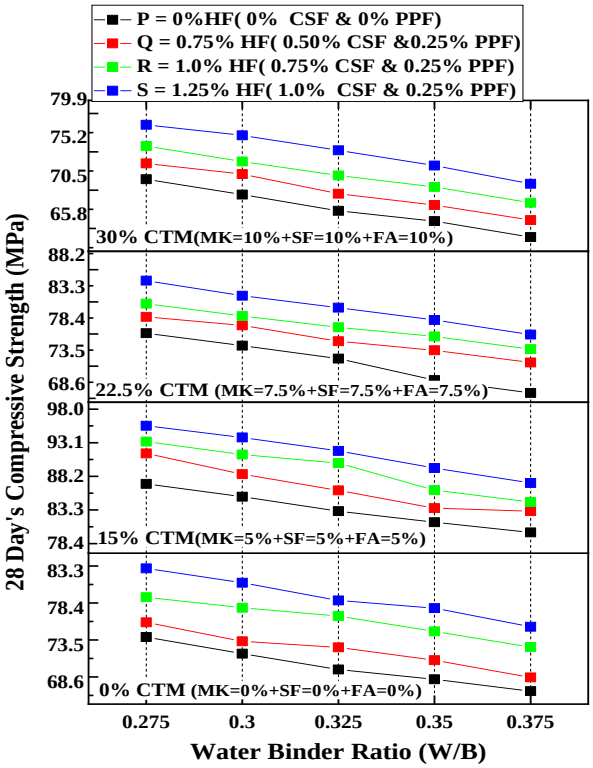

Fig. 5. Twenty-eight days Cube compression strength Vs. W/B ratio for HFRTHPC mix

3.1.1.2 Effect of Replacement Percentage of Cement by Combined Tertiary Mineral Admixture on Cube Compressive Strength of Tertiary Mineral Admixture Based HPC Mix with Hybrid-Fibers

To better understand the strength deviation caused by replacing cement with blended tertiary mineral admixtures in each mix, Figures 6 and 7 plot the cube compressive strengths for testing at 7 and 28 days for all water/binder ratios against the percentages of three combined mineral admixtures for various volumes of composite fibers. The correlation between the total percentages of tertiary mineral admixture and the 28-day cube compressive strength demonstrates that using a mixed tertiary mineral addition in place of cement increased the 28-day cube compressive strength. The addition of MK, SF, and FA enhances the mix's load-carrying capacity. The maximum cube compressive strength was obtained when 15% of the cement was replaced with mixed tertiary mineral additives across all composite materials. Beyond this 15% replacement, the compressive strength decreased. The CTM15SA1 mix outperformed the CTM0PA1 mix in 28-day cube compressive strength for high-fiber-reinforced high-performance concrete up to 29.49%. The fine mineral admixtures MK, SF, and FA, along with the filling of the interfacial transition zone with fine mineral admixture particles, generated pozzolanic reactions, which increased strength by up to 15% replacement due to the micro-filler effect [2,4,7,24]. At dosages greater than 15%, there was insufficient $Ca(OH)_2$ for the pozzolanic process, reducing the cube compressive strength as MK, SF, and FA then acted solely as fillers.

In comparing HPC mixes at a 20% replacement level, metakaolin in binary mixes achieved the highest compressive strength 91.70 MPa (A. gouda et al., 2022) [27], followed by silica fume 90.22 MPa (A. gouda et al., 2021) [25] and fly ash 87.40 MPa (A. gouda et al., 2020) [26]. The ternary mix of fly ash and silica fume improved strength to 92.32 MPa (S. Patil et al., 2021) [28]. However, the highest performance was observed in the tertiary blend of fly ash, metakaolin, and silica fume, reaching a compressive strength of 95.95 MPa. This superior performance is attributed to the synergistic effect of combining all three mineral admixtures, which enhances the concrete's microstructure through better particle packing, reduced porosity, and improved bonding, resulting in an overall increase in strength and durability.

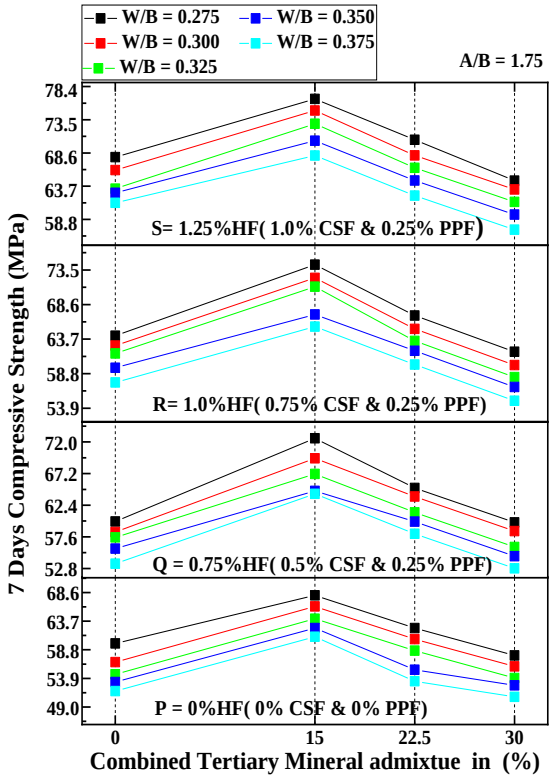

Fig. 6. Seven days cube compression strength Vs. % of combined tertiary mineral admixture

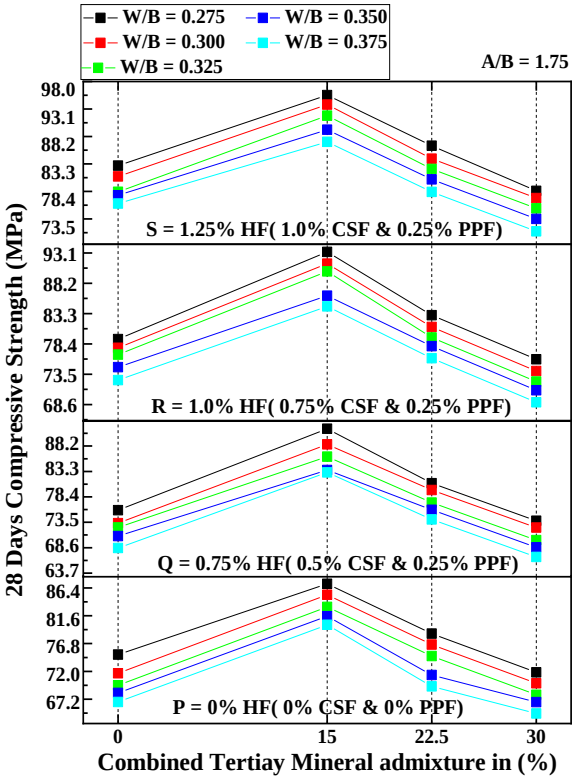

Fig. 7. Twenty-eight days cube compression strength Vs. % of combined tertiary mineral admixture

3.1.1.3 Effect of Composite Fiber Volume Percentage on Cube Compressive Strength of Tertiary Mineral Admixture Based HPC Mix with Hybrid-Fibers

Figs. 8 and 9 plot the cube compressive strengths against the volume percentages of composite fibers for various percentages of blended tertiary mineral admixture across different ages and water/binder ratios. This analysis aims to understand how composite fibers impact the compressive strength of each mix. The figures show that the compressive strength of the HFHPTC mix increases as the percentage of composite fibers is added. Specifically, the 28-day cube compressive strength improved with the addition of 0, 0.5, 0.75, and 1% CSF combined with a constant 0.25% PPF. This increase in cube compressive strength suggests a strong relationship between the fiber and the cement concrete matrix. The addition of composite fibers enhances the mixture, with the maximum cube compressive strength achieved at 1% CSF and 0.25% PPF for various amounts of mixed tertiary mineral admixture. For the PL0PA1 mix, the 28-day cube compressive strength increased by 23.89%, 26.49%, and 29.49% for the CTM15QA1, CTM15RA1, and CTM15SA1 mixes, respectively. The ability of these fibers to act as reinforcement at both macro and micro levels contributes to this performance. At the microscopic level, the fibers prevent the growth of microcracks, significantly influencing how microcracks form in the matrix. With more fibers in the matrix, the capacity for energy absorption increases, reducing the likelihood of micro and macro cracks forming and thus boosting the concrete's strength. While adding mono fibers to regular concrete enhances only ductility, the use of composite fibers and mixed mineral admixtures in this experiment significantly boosted the strength over plain HPC concrete due to the strain-hardening response of hybrid fiber-reinforced concrete [13-16, 18-22]. The greatest cube compressive strengths of the CTM15SA1 mix were 76.88 MPa and 95.68 MPa at 7 and 28 days, respectively

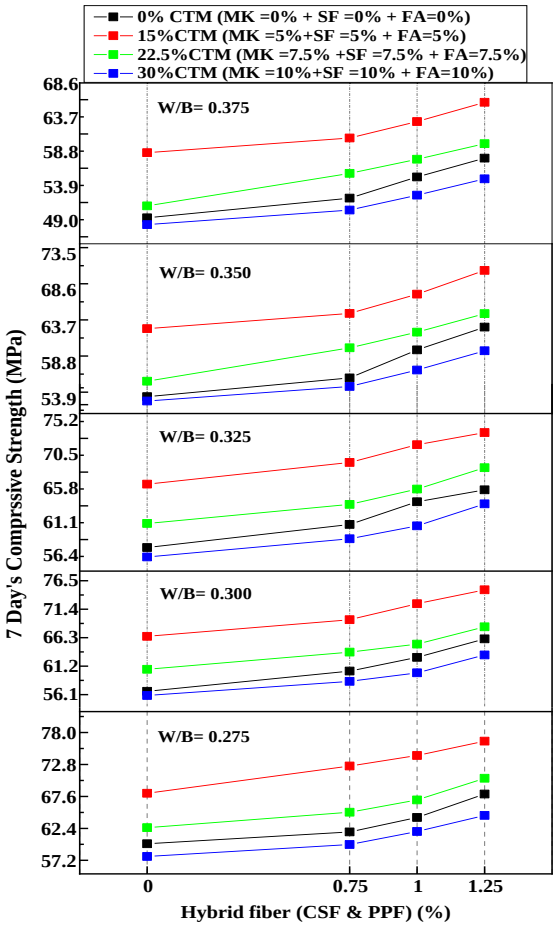

Fig. 8. 7 days Cube compressive strength Vs. volume % of composite fibers

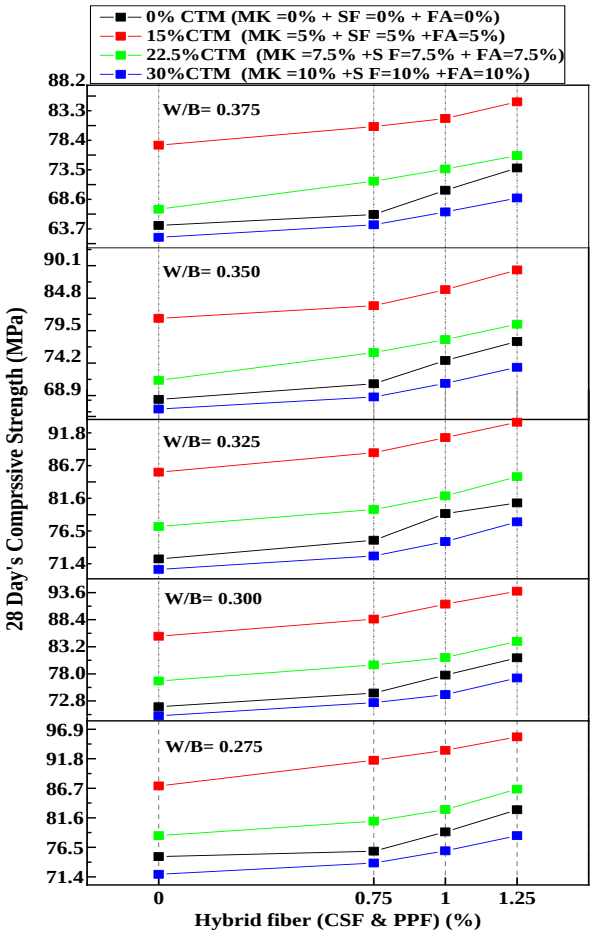

Fig.9. 28 days Cube compressive strength Vs. volume % of composite fibers

3.1.2 Split Tensile and Flexural Strength.

Figures 10 and 11 show the effect of replacing cement with varying percentages of combined tertiary mineral admixture on the 28-day curing split tensile and flexural strength. With a 15% replacement of cement by combined tertiary mineral admixture, the split tensile and flexural strengths of the mixture improved by 40.70% and 38.22% respectively, compared to the reference mix. For the CTM15SA1 mix, the highest split tensile and flexural strengths achieved were 7.04 MPa and 11.21 MPa respectively, indicating that 15% is the optimal substitution level. Beyond this percentage, insufficient availability of $Ca(OH)_2$ for the pozzolanic process reduces strength [2,4,24]. Figures 12 and 13 illustrate the effect of composite/hybrid fiber volume percentage on the split tensile and flexural strengths of high-performance concrete with blended tertiary mineral admixture. The load-carrying capacity of the mixture is enhanced by the inclusion of mixed steel and polypropylene fibers [13-16]. The current experiment shows that the greatest split tensile and flexural strengths were achieved with a combination of 1% crimped steel fiber and 0.25% polypropylene fiber, totalling a 1.25% hybrid fiber ratio.

In comparing split tensile and flexural strengths across HPC mixes at a 20% cement replacement level, the binary mix with metakaolin achieved the highest split tensile 7.0 MPa and flexural strengths 9.94 MPa (A. gouda et al., 2022) [27] among individual admixtures. However, the ternary mix of fly ash and silica fume offered only a slight improvement over other binary options, with split tensile and flexural strengths of 6.16 MPa and 9.12 MPa, S. (Patil et al., 2021) [28] respectively. The proposed tertiary mix, combining fly ash, metakaolin, and silica fume, delivered the most significant enhancements, reaching 7.04 MPa in split tensile strength and 11.21 MPa in flexural strength, the highest values in both categories.

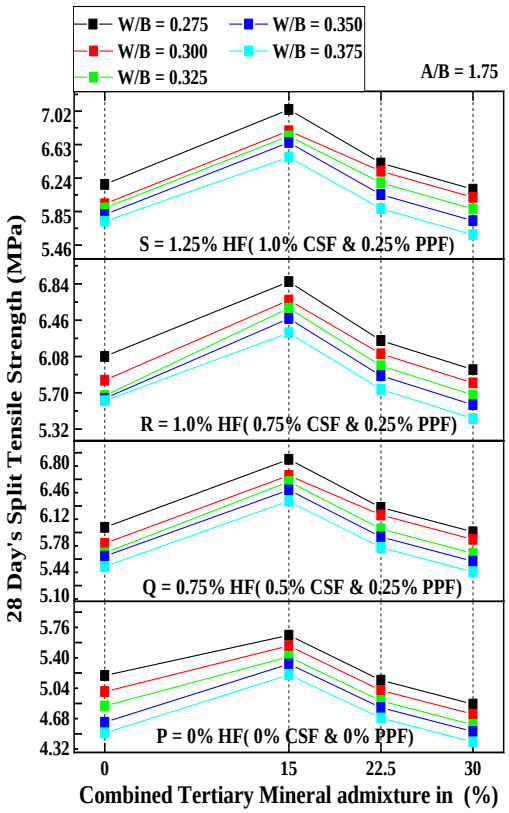

Fig. 10. Twenty-eight days Split Tensile strength Vs. % of combined tertiary mineral admixture

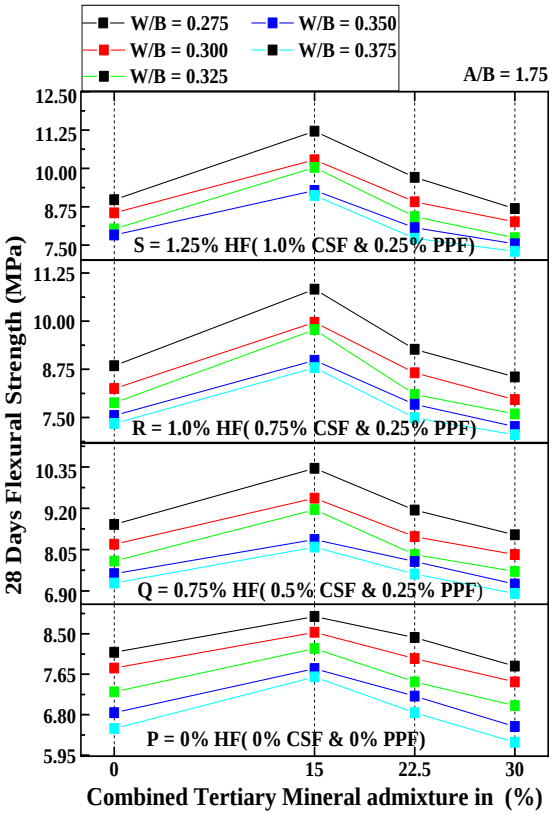

Fig. 11. Twenty-eight days Flexural strength Vs. % of combined tertiary mineral admixture

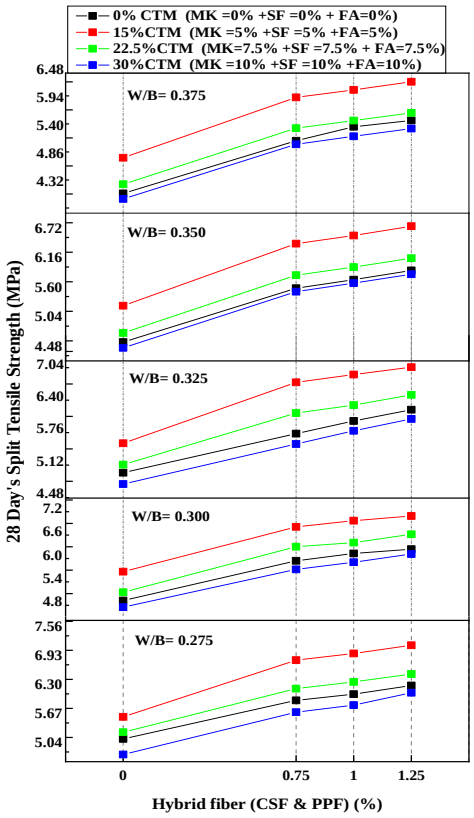

Fig. 12. Twenty-eight days Split Tensile strength Vs. volume % of composite fibers

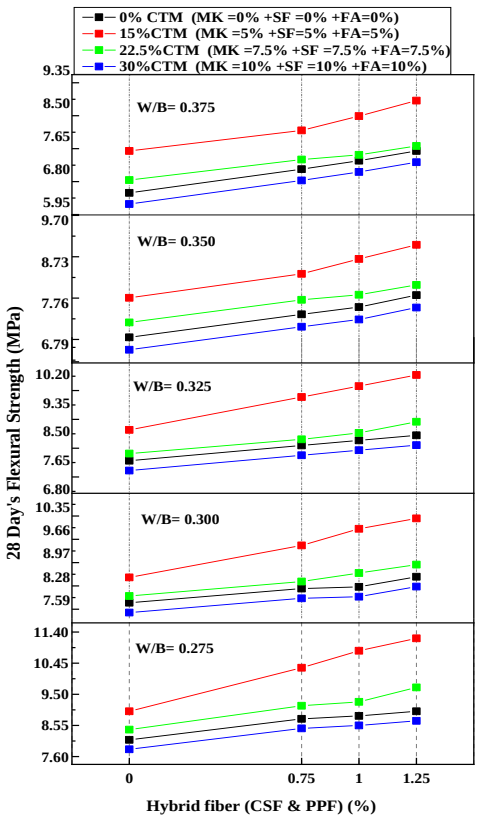

Fig.13. Twenty-eight days Flexural strength Vs. volume % of composite fibers.

3.1.3 The Inter-Relation Among Different Mechanical Properties of Tertiary Mineral Admixture Based HPC Concrete Mix with Hybrid Fibers

The interrelationships between cub compression strength and split-tensile strength, and cub compression strength and flexural strength, are depicted in Fig. 14 and Fig. 15 for specimens that were cured for 28 days. The formula $f_t = 0.7\sqrt{f_{ck}}$ MPa for normal concrete is prescribed by the BIS code IS:456-2000. This relationship was determined to be applicable for the hybrid fiber-reinforced tertiary blended HPC at 28 days of curing, the connection between split tensile strength and cub compressive strength was found to be $f_{ct} = 0.689\sqrt{f_{ck}}$ MPa, with a higher correlation value of 0.98756. Furthermore, a stronger correlation coefficient of 0.98588 was found for the link between cub compression strength and flexural strength for the hybrid fiber-reinforced tertiary mix at 28 days of curing, which is $f_r = 0.98\sqrt{f_{ck}}$ MPa.

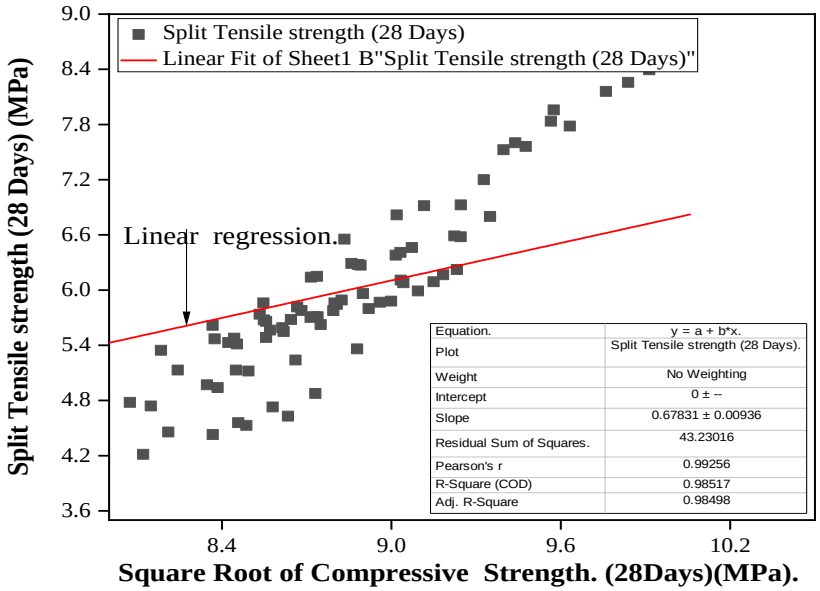

Fig. 14. Relationship between cube compression and split tension strength.

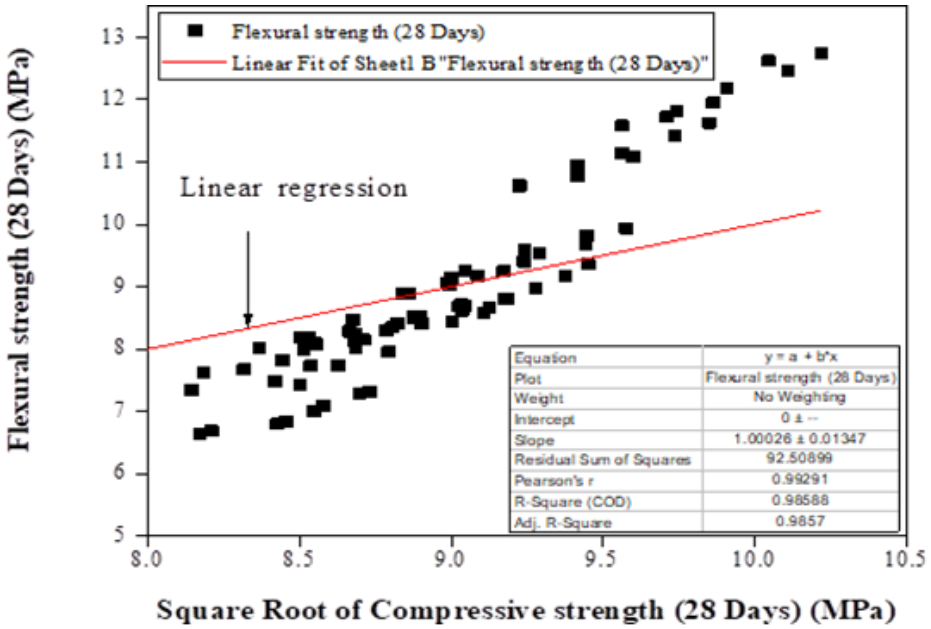

Fig. 15. Relationship between cube compression and flexural strength

3.2 Machine Learning Approach

The AdaBoost regressor was used to estimate the compressive strength of HFRTHPC, as illustrated in Fig. 16, which compares predicted and actual results. The model had an R-squared score of 0.903 for the training datasetand 0.897 for the test dataset. Despite its performance, with MAE = 0.6884, MSE = 0.8388, and RMSE = 0.9998 (Table 5), the errors appear to be outside the intended range when compared to other methods. The error distribution map in Fig. 17 shows the differences between the anticipated and practical results of HFRTHPC compressive strength using AdaBoost. Notably, the cumulative error estimates continue to be below 6 MPa. We recorded a maximum error of 5.72 MPa, a minimum error of 0.25 MPa, and an average error of 2.64 MPa.

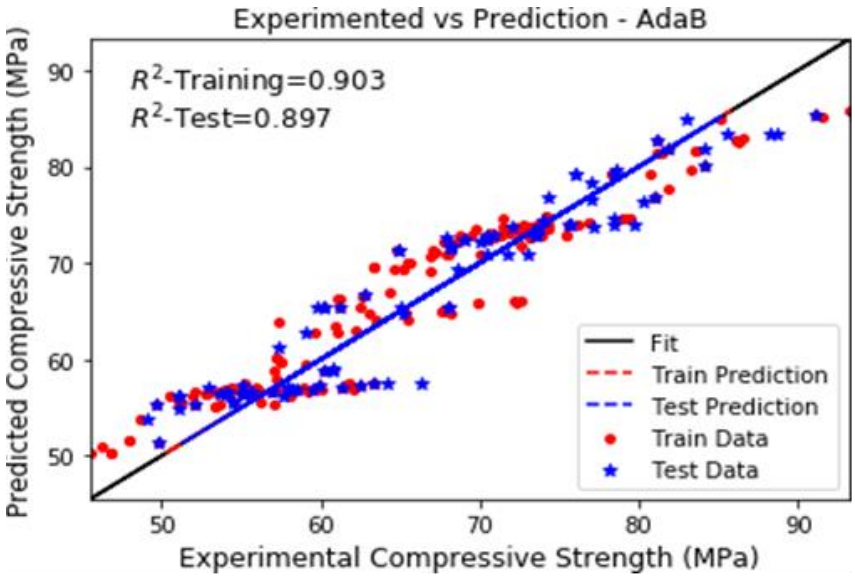

Fig. 16. Predicted V/s Experimental results for HFRTHPC CS – AdaB model

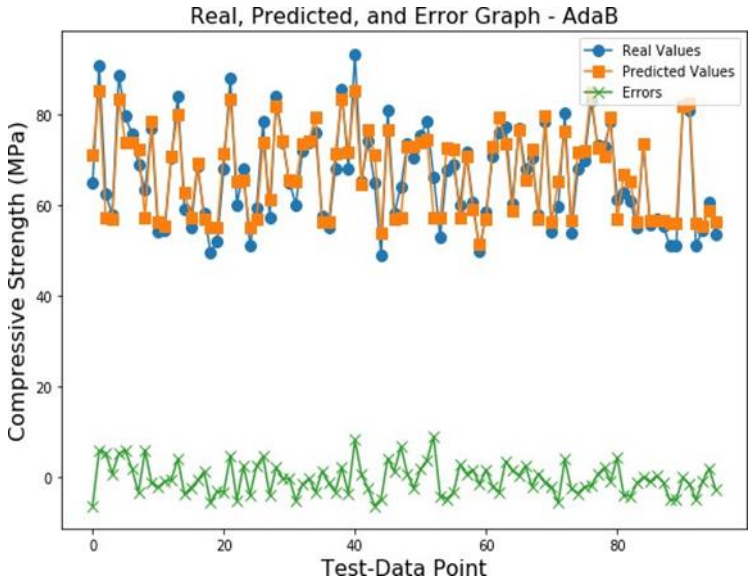

Fig. 17. Real, Predicted and Error distribution for AdaB model

Regression between the anticipated values and experimental values for HFRTHPC was conducted by adopting the RF algorithm, as illustrated in Fig.18. The RF shows less error variance and better-estimated outcomes than AdaB. The adequacy of the RF model is represented by an acceptable R2 value for training and testing of 0.997 and 0.962, respectively, and MAE = 0.4247, MSE = 0.420, and RMSE = 0.648. The error distribution of RF predicted and experimental for HFRTHPC compressive strength is illustrated in Fig.19.The total error values are below 6 MPa. Based on this distribution, the highest, lowest, and average values are 5.788, 0.032, and 1.546 MPa, respectively. As a result, the RF prediction findings are more precise than the AdaB model.

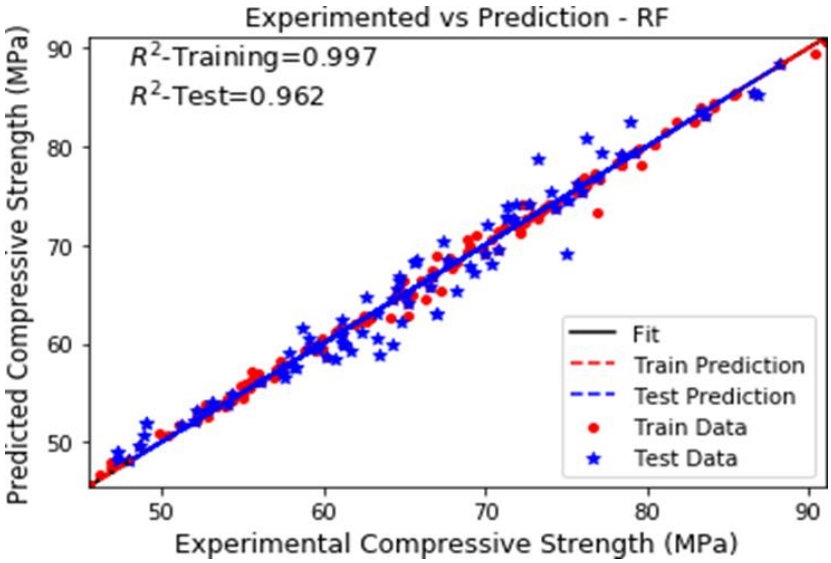

Fig. 18. Predicted V/s Experimental results for HFRTHPC CS – RF

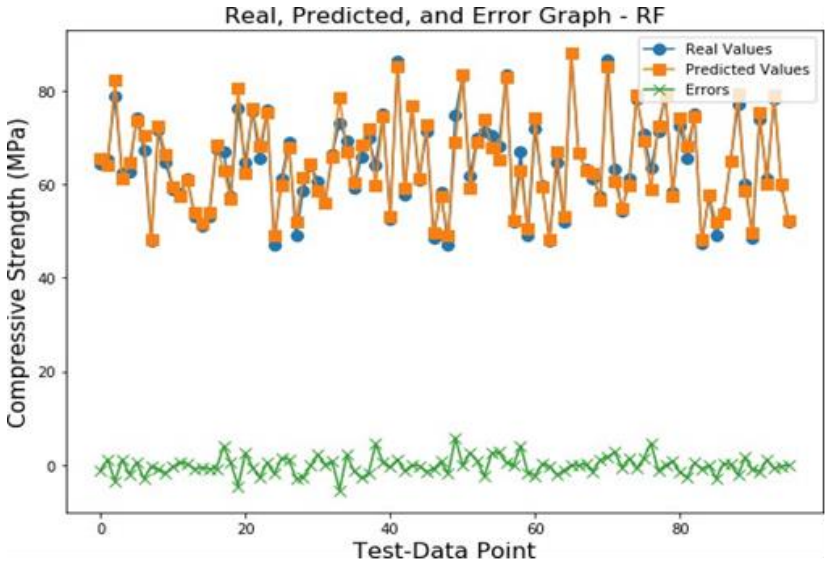

Fig. 19. Real, Predicted and Error distribution for RF model

Fig. 20 and Fig. 21 depicts the predicted results and error pattern representing the expected and experimental results for the compressive strength of HFRTHPC. Based on this distribution, the highest, lowest, and mean values are 4.004, 0.002, and 0.613 MPa, respectively. The cumulative error values are below 5 MPa. The XGB model demonstrates more precision, as seen by its higher R2 and lower error values. In contrast, the obtained XGB models' R2 and error values are adequate. Therefore, the finding suggests that the precision of XGB prediction results surpasses that of AdaB and RF models illustrates the anticipated and empirical results pertaining to the cub compressive strength of high-performance concrete reinforced with mixed fibers, as determined through the utilization of XGB. The R2 value training and test data sets are 1.000 and 0.994, respectively, and MAE = 0.0108, MSE = 0.0004, and RMSE = 0.0212 show highly precise results with better accuracy. At the same time, the estimated outcomes for HFRTHPC compressive strength are in the adequate.

The presented Fig. 22 illustrates the anticipated and empirical results pertaining to the split tensile strength of high-performance concrete reinforced with composite fibers, utilizing the AdaBoost algorithm. The R^2 values fortraining and testing are 0.924 and 0.912, respectively.

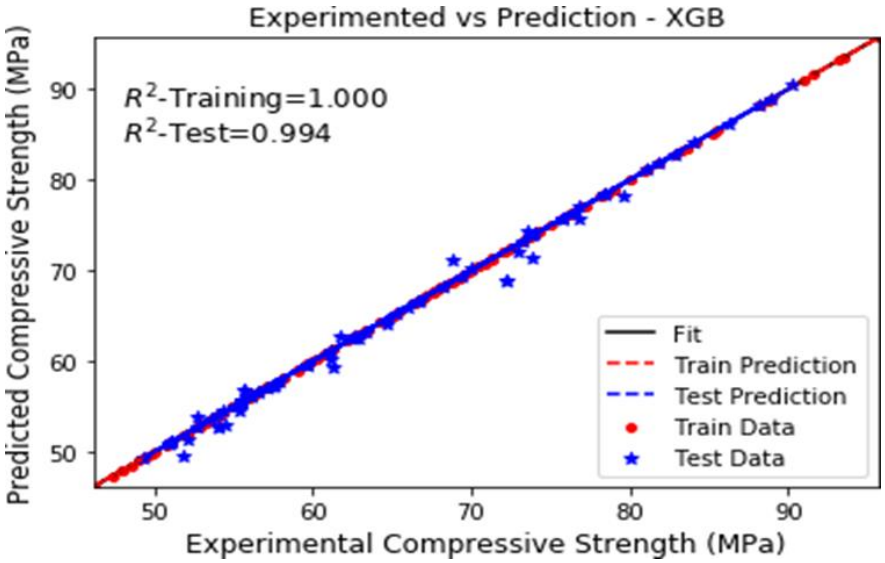

Fig. 20. Predicted V/s Experimental results for HFRTHPC CS – XGB model

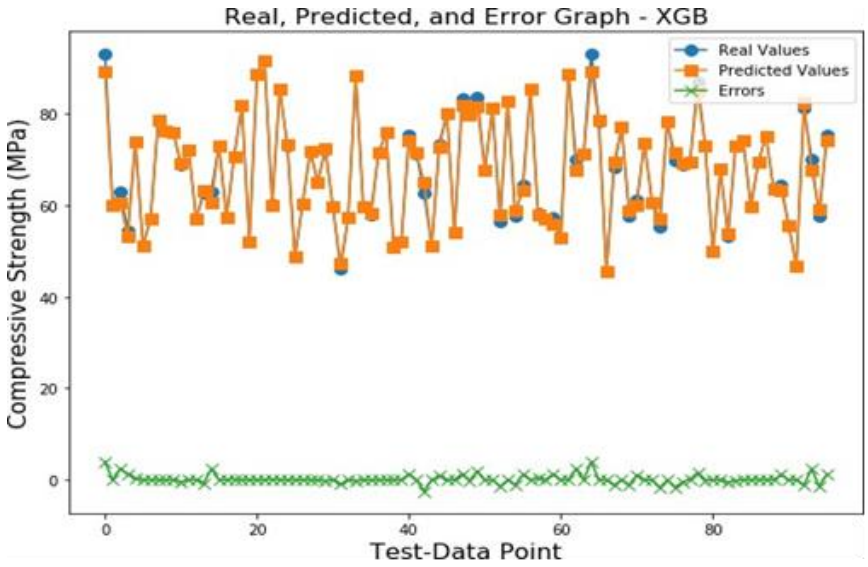

Fig. 21. Real, Predicted and Error distribution for XGB model

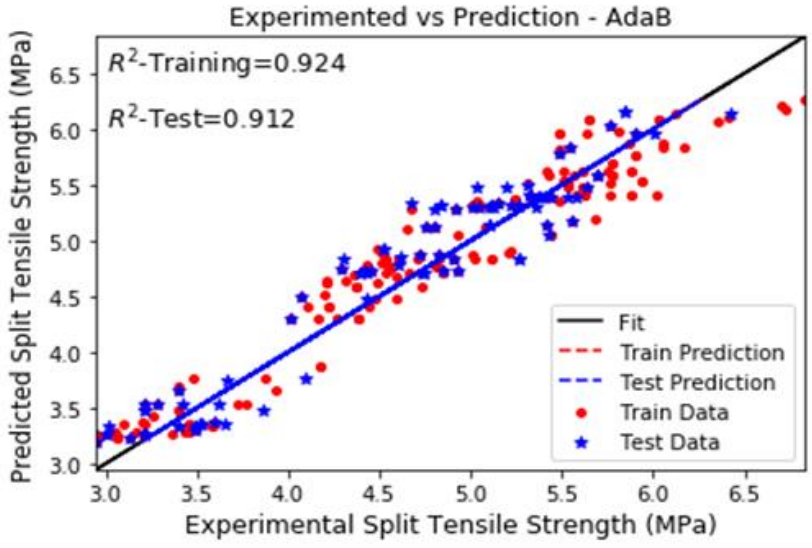

Fig. 22. Predicted V/s Experimental results for HFRTHPC TS – AdaB model

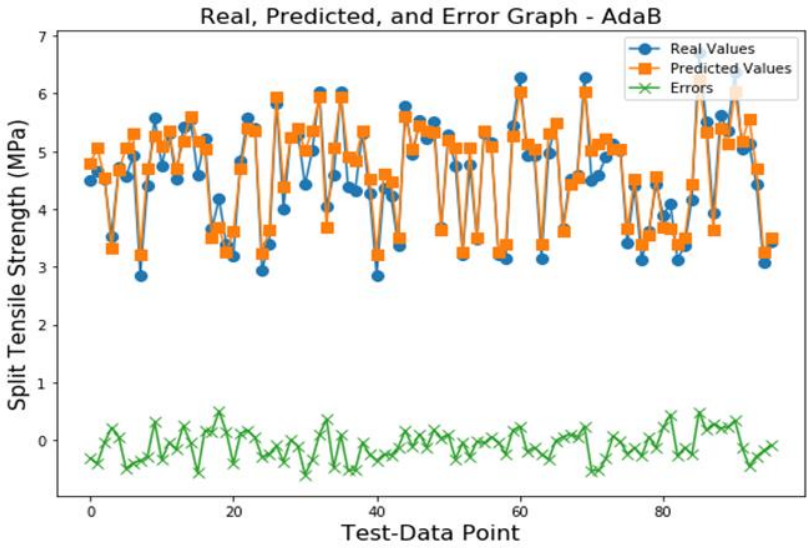

Fig. 23. Real, Predicted and Error distribution for AdaB model

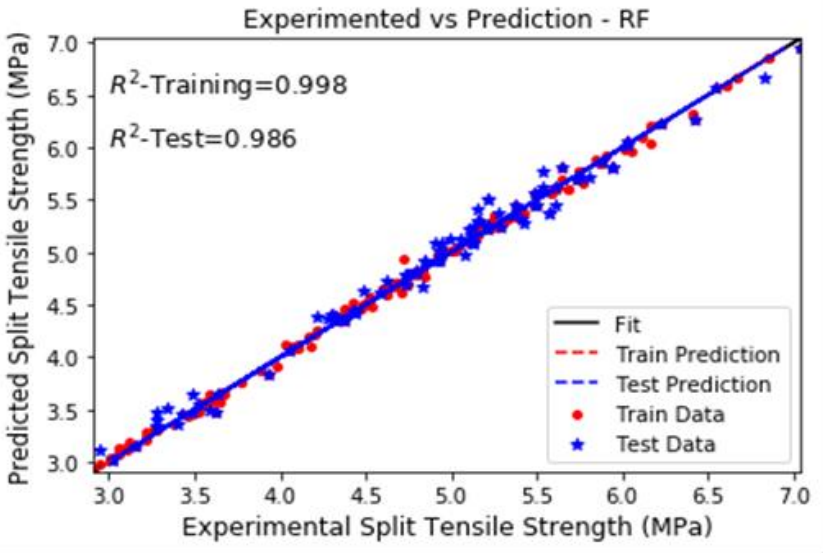

Fig .24. Predicted V/s Experimental results for HFRTHPC TS – RF model

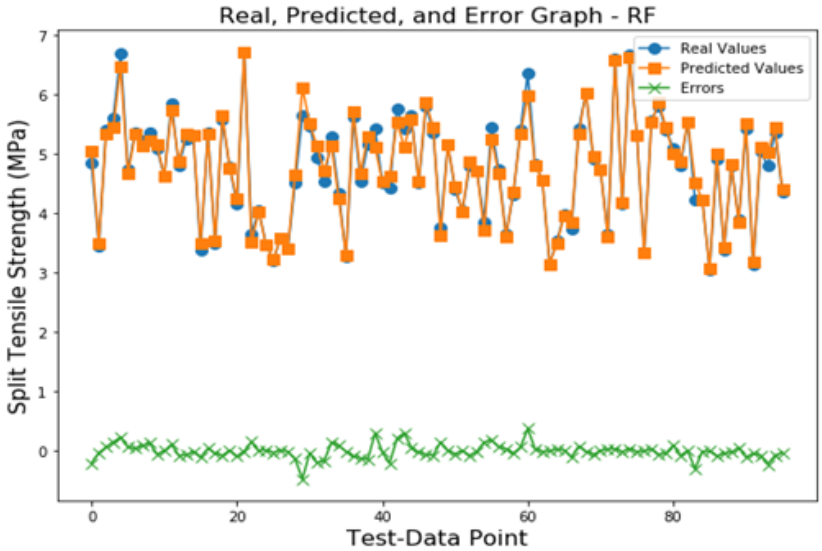

Fig. 25. Real, Predicted and Error distribution for RF model

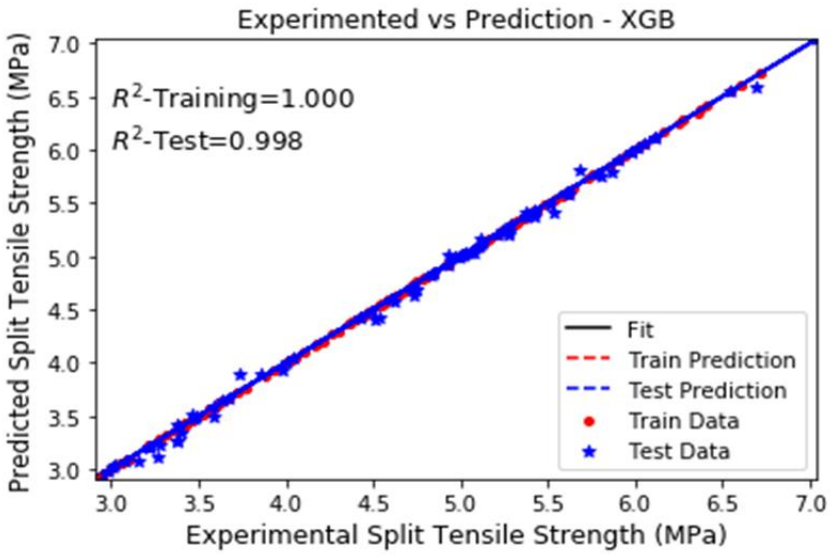

Fig. 26. Predicted V/s Experimental results for HFRTHPC TS – XGB model

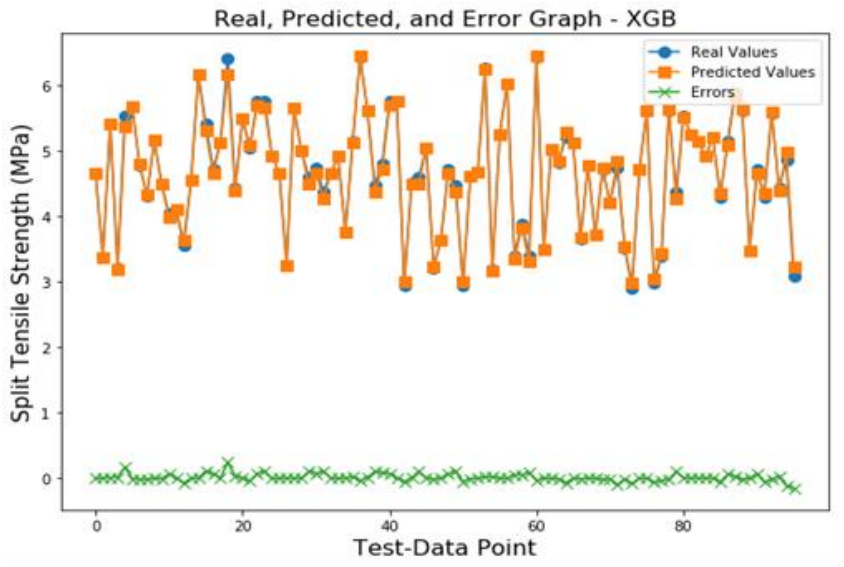

Fig. 27. Real, Predicted and Error distribution for XGB model

The MAE = 0.1921, MSE = 0.0568, and RMSE = 0.2384 confirm that AdB was unable to make reasonable predictions of tensile strength. Fig. 23 illustrates the errors between predicted and experimental values of split tensile strength via AdB. The minimum error was 0.008 MPa, the maximum error was 0.503 MPa, and the average error was 0.186 MPa in the AdB prediction. Figs. 24 and Fig. 25 indicate the predicted and experimental split tensile strength for composite fiber-reinforced tertiary blended high-performance concrete using RF and the errors between the experimental and estimated results using RF, respectively. The R^2 = 0.998 (training), R^2 = 0.986 (test), MAE = 0.0301 MPa, MSE = 0.0618 MPa, and RMSE = 0.0434 MPa in RF, showing the minimum errors in both AdB and RF. RF was more precise than AdB in the prediction of split tensile strength. The maximum and minimum error between practical and anticipated split tensile strength results using RF were 0.3754, 0.0008 MPa, and 0.0928, respectively.

Split tensile strength has been predicted using the XGB algorithm. The R^2 = 1.000 (training), R^2 = 0.998 (test), MAE = 0.0033 MPa, MSE = 0.02757 MPa, and RMSE = 0.0051 MPa using this algorithm show that XGB was more accurate than RF and AdB in predicting tensile strength. Fig. 26. Experimental and anticipated values and error distribution for XGB and Fig. 27 showed that the maximum and minimum errors were 0.24 MPa, 0.0001 MPa, and an average error of 0.049 MPa, respectively.

Fig. 28 presents the results of the AdB algorithm in predicting the HFRTHPC flexural strength. The AdB approach is estimated to have a moderate level of accuracy and divergence among experimental and estimated findings. The R^2 of 0.916 (training) and 0.894 (test) suggests that the AdB method for calculating the HFRTHPCflexural strength is satisfactory, and the experimental and predicted results reasonably agree. The error values MAE = 0.3933, MSE = 0.2204, and RMSE = 0.4695 are not in the adequate range for the remaining algorithm. Fig. 29 presents the actual, estimated, and error values distribution for the AdB model, and the maximum and minimum errors were 1.072 MPa, 0.008 MPa, and an average error of 0.367 MPa, respectively. The analysis of errors indicated that the AdaB model was estimated reasonably.

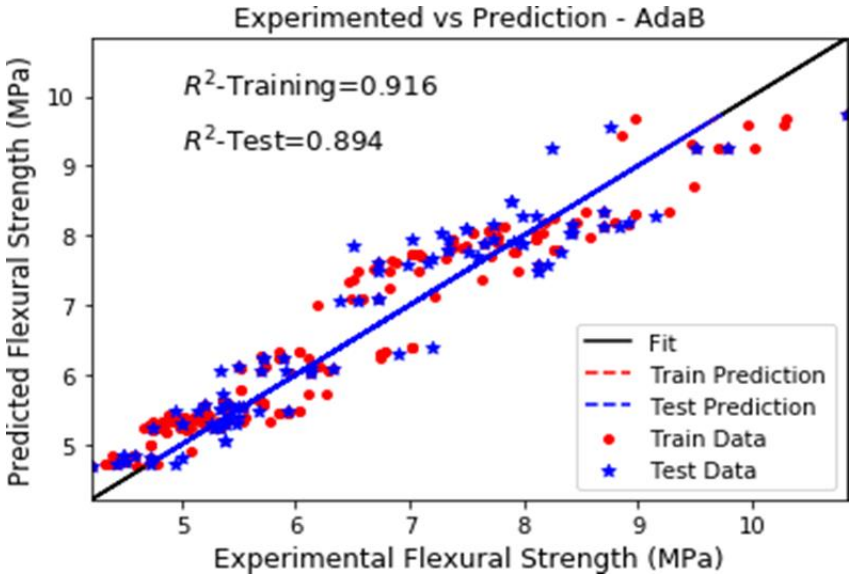

Fig. 28. Predicted V/s Experimental results for HFRTHPC FS – AdaB model

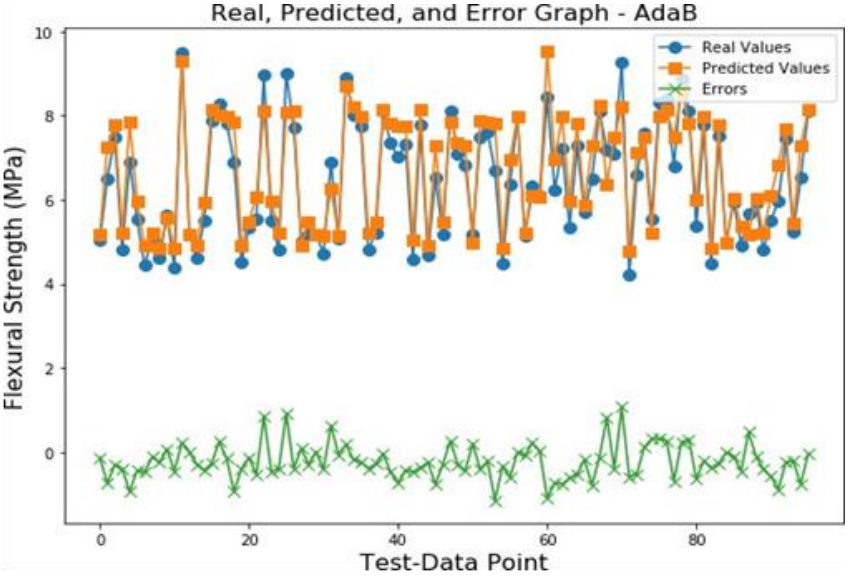

Fig. 29. Real, Predicted and Error distribution for AdaB model

Fig. 30 illustrates the correlations between the estimated and observed flexural strength values of HFRTHPC. This relationship provides 0.996 (training) and 0.982 (test) as the determination coefficient (R^2) values, as well as MAE = 0.0511 MPa, MSE = 0.0082 MPa, and RMSE = 0.0796 MPa. It is important to mention that the vertical axis represents the anticipated values, while the horizontal axis represents the experimental data for flexural strength. Fig. 31 shows the difference between the actual and predicted outcomes.

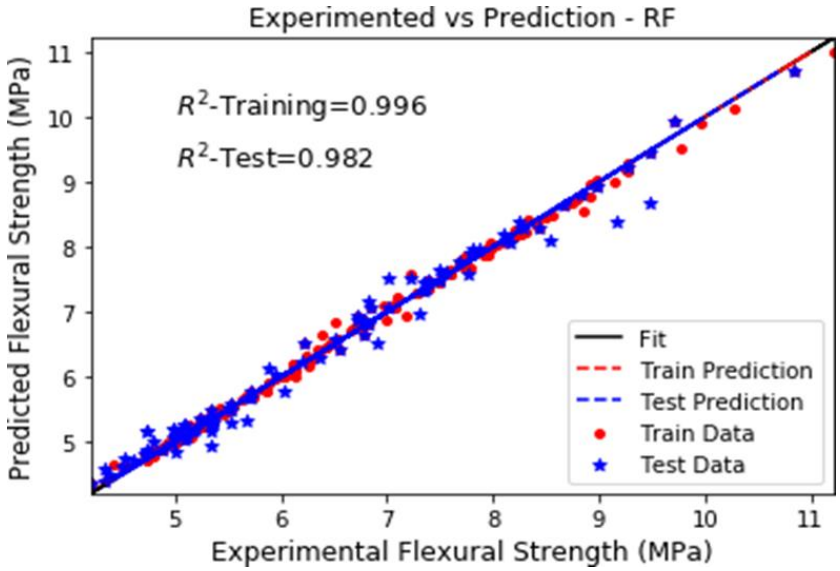

Fig. 30. Predicted V/s Experimental results for HFRTHPC FS – RF model

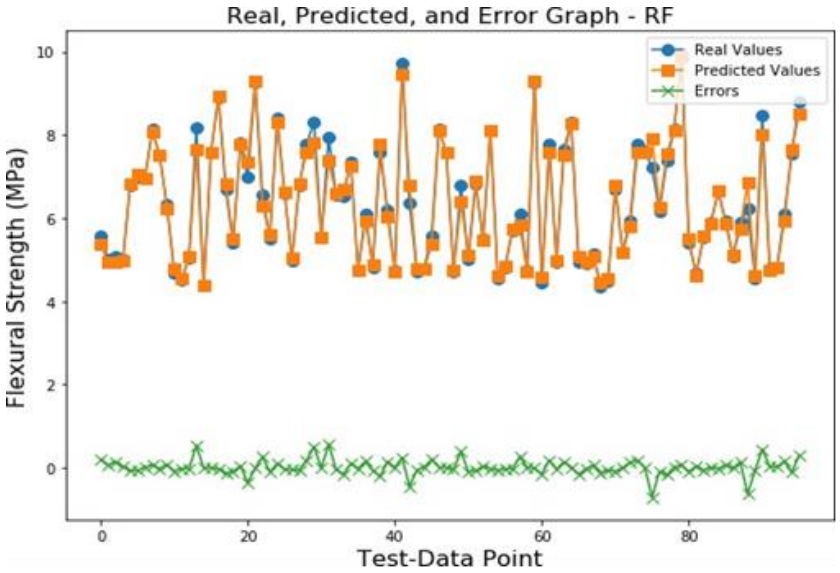

Fig. 31. Real, Predicted and Error distribution for RF model

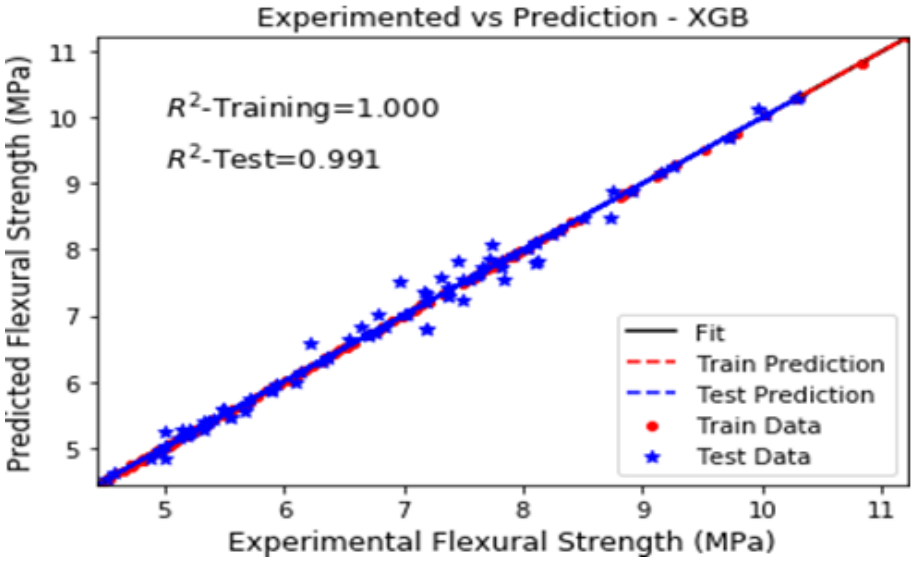

Fig. 32. Predicted V/s Experimental results for HFRTHPC FS – XGB model

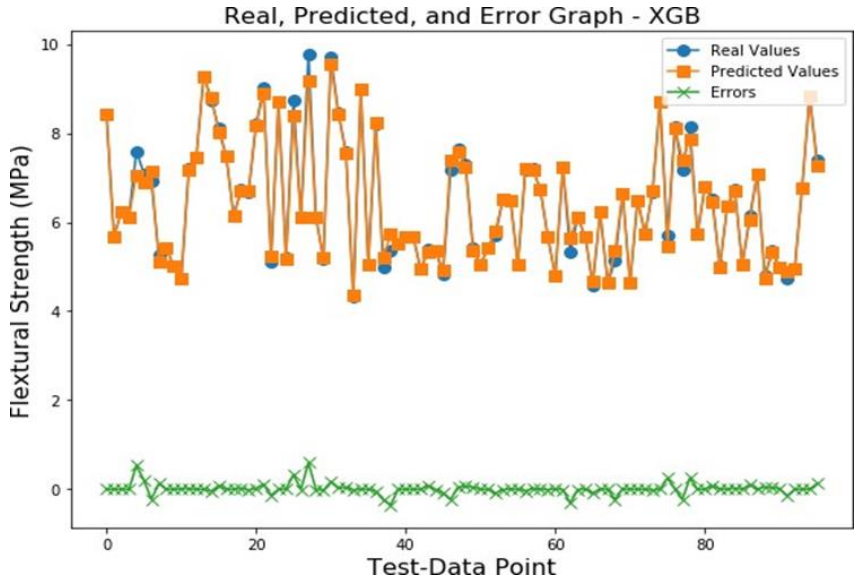

Fig. 33. Real, Predicted and Error distribution for XGB model

Here, the horizontal axis depicts the dataset for testing, whereas the anticipated flexural strength results are shown on the vertical axis. The difference shows the higher values, i.e., 0.574 MPa, the lower values, i.e., 0.003 MPa, and the average values, i.e., 0.145 MPa. Moreover, it has been determined that the total error values are below 1 MPa. Fig. 32 depicts that the XGB model offers a more precise relationship between the practice and anticipated HFRTHPC flexural strength results, which results in R^2 = 1.00 (training), R^2 = 0.991 (test), MAE = 0.025 MPa, MSE = 0.0063 MPa, and RMSE = 0.0042 MPa. The vertical and horizontal axes show expected and experimental flexural strength values. Fig. 33 shows the data distribution, showing actual versus projected outcomes. Here, the horizontal axis depicts the dataset for testing the models, whereas the anticipated flexural strength results are deciphered on the vertical axis. Based on this distribution, the highest, lowest, and average values are 0.599, 0.0001, and 0.0073 MPa, respectively. It is also found that total error values are below 01MPa.

Table 7. Statistical evaluation for the models

Models			AdaB	RF	XGB
	R^2	Training	90.3	99.7	100
		Test	89.7	96.2	99.4
Compressive Strength	MAE		0.6884	0.4247	0.0108
	MSE		0.8388	0.42	0.0004
	RMSE		0.9998	0.648	0.0212
	R^2	Training	92.4	99.8	100
		Test	91.2	98.6	99.8
Split Tensile Strength	MAE		0.1921	0.0301	0.0033
	MSE		0.0568	0.0618	0.02757
	RMSE		0.2384	0.0434	0.0051
	R^2	Training	91.6	99.6	100
		Test	89.4	98.2	99.1
Flexural Strength	MAE		0.3933	0.0511	0.025
	MSE		0.2204	0.0082	0.0063
	RMSE		0.4695	0.0796	0.0042

In contrast to the AdaB approach, the RF model produced more accurate results and the minimum difference between actual and estimated findings. Since the RF model had a smaller deviation of errors and was more accurate than the AdaB model, as a result of the usage of an endless number of decision trees during training and its initial decision tree's emphasis on incorrectly categorized input, the RF model achieves better accuracy. Another model also makes use of the same data. This

process is repeated until a sufficient number of basic learners have been created. The error distribution demonstrated that the XGB model outperformed the RF and AdaB models. The performance of the other models used is also satisfactory. The XGB model is more precise because it employs a tree-based ensemble learning strategy that optimizes output by generating sub models.

Fig. 34 shows the evaluation of predictive models for compressive strength. AdaB, RF, and XGB all demonstrated commendable performance across both training and test datasets. Notably, XGB emerged as the top performer, consistently surpassing AdaB and RF. With flawless R^2 scores of 100% on both training and test datasets, XGB showcased exceptional predictive capabilities. Moreover, its superiority was further evidenced byachieving the lowest error metrics (MAE, MSE, and RMSE) compared to AdaB and RF. These findings underscore XGB's remarkable accuracy and precision in forecasting compressive strength, positioningit as the preferred model for such predictions.

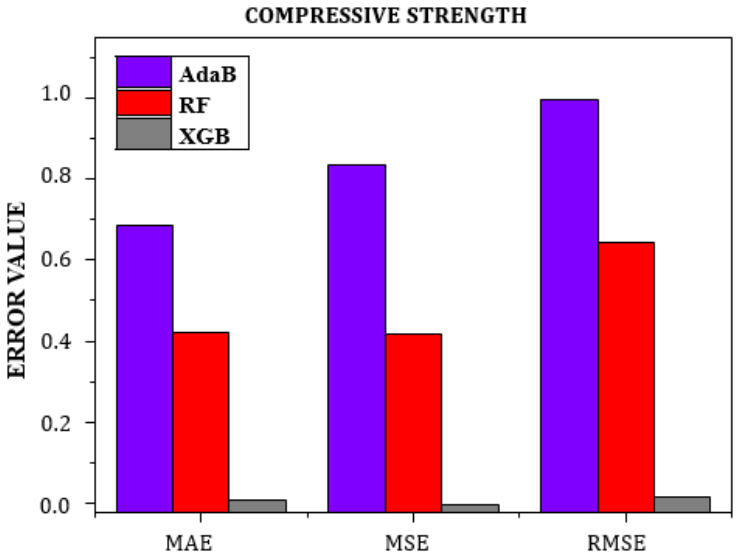

Fig. 34. Error analysis- Compressive strength

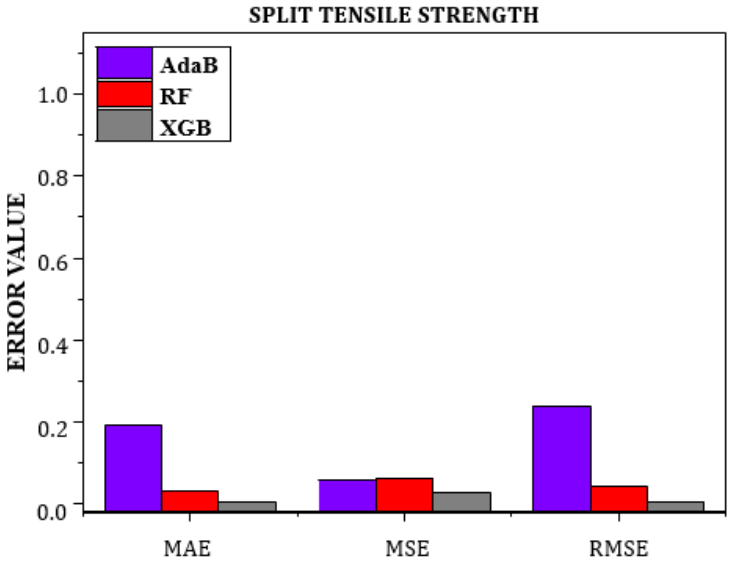

Fig. 35. Error analysis- Tensile strength

Fig. 35 depicts assessing the predictive models for tensile strength. AdaB, RF, and XGB each demonstrated commendable performance. However, XGB consistently emerged as the standout performer. Impressively, XGBattained perfect R^2 scores of 100% on both training and test datasets,

indicating its exceptional predictive prowess. Furthermore, XGB showcased the lowest error metrics (MAE, MSE, and RMSE) compared to AdaB and RF, underscoring its unmatched accuracy and precision in predicting tensile strength.These findings emphasize XGB's superiority and its potential as the preferred model for such predictive tasks.

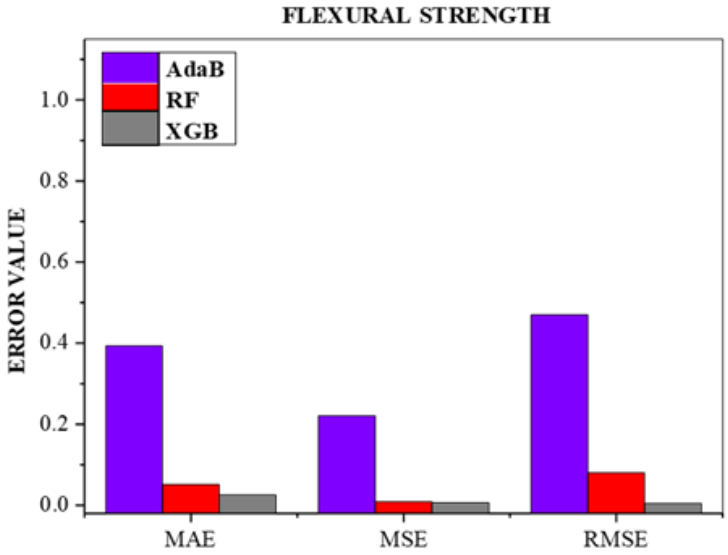

Fig. 36. Error analysis- Flexural strength

Fig. 36 represents the evaluation of predictive models for flexural strength. All models demonstrated satisfactory performance; however, XGB emerged as the standout performer. Remarkably, XGB attained perfect R^2 scores of 100% on both training and test datasets, showcasing its exceptional predictive capabilities. Additionally, XGBexhibited the lowest error metrics (MAE, MSE, and RMSE) compared to other models, indicating superior accuracy and precision in predicting flexural strength. These findings underscore XGB superiority and highlight its potential as the preferred model for accurate predictions of flexural strength in practical applications.

4. Conclusions

- The study successfully demonstrates that the incorporation of hybrid fibers (crimped steel fibers and polypropylene fibers) significantly enhances the mechanical properties of concrete. The optimal mix identified includes 1% crimped steel fiber and 0.25% polypropylene fiber.
- A notable increase in compressive strength of up to 30.24% was achieved with the Hybrid Fiber-Reinforced Tertiary Blended High-Performance Concrete (HFRTHPC) mix compared to the reference mix, with the highest compressive strength recorded at 28 days.
- The study revealed that as the W/B ratio increased from 0.275 to 0.375, the compressive strength of the HFRTHPC mix decreased. The highest strengths were consistently observed at the lowest W/B ratio, confirming the importance of maintaining a low W/B ratio for high-performance concrete.
- The results indicate a substantial improvement in split tensile strength (up to 40.70%) and flexural strength (up to 38.22%) when 15% of the Ordinary Portland Cement (OPC) is replaced with combined tertiary mineral admixtures (silica fume, metakaolin, and fly ash).
- Among the mixtures analysed, the Hybrid Fiber-Reinforced Tertiary Blended High-Performance Concrete (HFRTHPC) demonstrated optimal performance at a hybrid fiber volume of 1.25% with a 15% addition of combined mineral admixture. This combination led to significant improvements in compressive, splitting tensile, and flexural strength compared to the reference mix, highlighting the effectiveness of this hybrid approach.
- The proposed tertiary mix of cement with mineral admixtures outperformed other configurations, such as binary and ternary mixes, due to the combined benefits of fly ash,

metakaolin, and silica fume, which enhance particle packing, reduce porosity, and improve bonding in the concrete matrix.

- The research successfully applied three machine learning techniques—AdaBoost, Random Forest, and Extreme Gradient Boost—to model the mechanical properties of concrete. Among these, the Extreme Gradient Boost (XGB) model exhibited superior predictive accuracy and generalization capabilities, achieving R^2 scores of 1.000 for both training and testing datasets for compressive strength. This indicates the potential of machine learning as an effective tool for predicting concrete properties.
- This research highlights the potential for optimizing concrete compositions to create more sustainable construction materials, reducing the environmental impact associated with traditional concrete production by effectively utilizing industrial by-products like silica fume, metakaolin, and fly ash.
- The findings of this study provide a foundation for future research into hybrid fiber-reinforced concrete, suggesting avenues for further exploration in the optimization of fiber types, dosages, and the incorporation of additional sustainable materials.

References

[1] Patel V, Shah N. A survey of high-performance concrete developments in civil engineering field. Open J Civil Eng. 2013;3(2):69-79. https://doi.org/10.4236/ojce.2013.32007

[2] Juenger MCG, Siddique R. Recent advances in understanding the role of supplementary cementitious materials in concrete. Cem Concr Res. 2015;10:1016. https://doi.org/10.1016/j.cemconres.2015.03.018

[3] Dave N, Misra AK, Srivastava A, Kaushik SK. Experimental analysis of strength and durability properties of quaternary cement binder and mortar. Constr Build Mater. 2016;12:195. https://doi.org/10.1016/j.conbuildmat.2015.12.195

[4] Khan SU, Nuruddin MF, Ayub T, Shafiq N. Effects of different mineral admixtures on the properties of fresh concrete. Sci World J. 2014;1:986567. https://doi.org/10.1155/2014/986567

[5] Gesoğlu M, Güneyisi E, Özbay E. Properties of self-compacting concretes made with binary, ternary, and quaternary cementitious blends of fly ash, blast furnace slag, and silica fume. Constr Build Mater. 2009;23(5):1847-54. https://doi.org/10.1016/j.conbuildmat.2008.09.015

[6] Dhrangadharia S, Vishwakarma S, Kumar A, Saran B. Effect of quaternary binder systems on mechanical properties of concrete. Int J Eng Sci Res. 2018;6(1):2347-6532.

[7] Kathirvel P, Saraswathy V, Karthik SP, Sekar ASS. Strength and durability properties of quaternary cement concrete made with fly ash, rice husk ash, and limestone powder. Arab J Sci Eng. 2012;38(3):589-98. https://doi.org/10.1007/s13369-012-0331-1

[8] Makhloufi Z, Bouziani T, Hadjoudja M, Bederina M. Durability of limestone mortars based on quaternary binders subjected to sulfuric acid using drying-immersion cycles. Constr Build Mater. 2014;71:579-88. https://doi.org/10.1016/j.conbuildmat.2014.08.086

[9] Soroushian P, Khan A, Hsu JW. Mechanical properties of concrete materials reinforced with polypropylene or polyethylene fibers. ACI Mater J. 1992;89(6):535-40. https://doi.org/10.14359/4018

[10] Pierre P, Pleau R, Pigeon M. Mechanical properties of steel microfiber reinforced cement pastes and mortars. J Mater Civil Eng. 1999;11(4):317-24 https://doi.org/10.1061/(ASCE)0899-1561(1999)11:4(317)

[11] Jain A, Singh B, Shrivastava Y. Investigation of kerf deviations and process parameters during laser machining of basalt-glass hybrid composite. J Laser Appl. 2019;31(3):032017. https://doi.org/10.2351/1.5111369

[12] Anandan S, Alsubih M. Post-elastic deformation characteristics of hybrid fiber reinforced concrete composites. Lat Am J Solids Struct. 2020;17(1):1-20. https://doi.org/10.1590/1679-78255851

[13] Sharma KK, Shrivastava Y, Neha E, Jain A, Singh B. Evaluation of flexural strength of hybrid FRP composites having three distinct laminates. Mater Today Proc. 2020;38:418-22. https://doi.org/10.1016/j.matpr.2020.07.599

[14] Zhong H, Zhang M. Experimental study on engineering properties of concrete reinforced with hybrid recycled tyre steel and polypropylene fibres. J Clean Prod. 2020;259:120914. https://doi.org/10.1016/j.jclepro.2020.120914

[15] Eidan J, Rasoolan I, Poorveis D, Rezaeian A. Effect of polypropylene short fibers on energy absorption capacity and durability of concrete. J Test Eval. 2020;49(5):1-8. https://doi.org/10.1520/JTE20190778

[16] Afroughsabet V, Ozbakkaloglu T. Mechanical and durability properties of high-strength concrete containing steel and polypropylene fibers. Constr Build Mater. 2017;94:73-82. https://doi.org/10.1016/j.conbuildmat.2015.06.051

[17] Gupta AK. Experimental studies of strength and durability analysis of concrete incorporating ultrafine slag [doctoral dissertation]. Solan (HP): Jaypee Univ Inf Technol; 2018.
[18] Annadurai A, Ravichandran A. Strength prediction of hybrid fiber reinforced high strength concrete. Int J ChemTech Res. 2015;8(12):675-81.
[19] Alavi Nia A, Hedayatian M, Nili M, Sabet VA. An experimental and numerical study on how steel and polypropylene fibers affect the impact resistance in fiber-reinforced concrete. Int J Impact Eng. 2012;46:62-73. https://doi.org/10.1016/j.ijimpeng.2012.01.009
[20] Murali G, Santhi AS, Ganesh GM. Impact resistance and strength reliability of fiber reinforced concrete using two-parameter Weibull distribution. J Eng Appl Sci. 2014;9(4):554-59.
[21] Nagaraja K, Sudarshan Rao H, Shiva Shankar Reddy T. Study on performance of ternary blended high-strength hybrid fiber reinforced concrete. Int J Civil Eng Technol. 2018;9(11):925-33.
[22] Sreenu R, Hajarath K, Madhukar M. An experimental study on performance of ternary blended high-strength fiber reinforced concrete. Int Res J Eng Technol. 2018;5(8):1-7.
[23] Malagavelli V, Angadi S, Prasad JSR, Joshi S. Influence of metakaolin in concrete as partial replacement of cement. Int J Civil Eng Technol. 2018;9(7):105-11.
[24] Liu G, Guo Y, Li Q, Wang L. The threshold value of effective replacement ratio of fly ash mortar based on amount of calcium hydroxide. IOP Conf Ser Earth Environ Sci. 2020;455(1):012125. https://doi.org/10.1088/1755-1315/455/1/012125
[25] Gouda A, Somasekharaiah HM. Strength and durability studies on hybrid fiber reinforced high-performance concrete for silica fume-based mineral admixture. IOP Conf Ser Earth Environ Sci. 2021;822(1):012041. https://doi.org/10.1088/1755-1315/822/1/012041
[26] Gouda A, Somasekharaiah HM, Mallikarjuna HM. Mechanical properties and acid attack test of hybrid fiber reinforced high-performance concrete for fly ash-based mineral admixture. Mater Today. 2022;51:742-49. https://doi.org/10.1016/j.matpr.2021.06.220
[27] Gouda A, Somasekharaiah HM, Mallikarjuna HM. Combined effect of metakaolin and hybrid fibers on the strength properties of high-performance concrete. Mater Today. 2022;49:1527-36. https://doi.org/10.1016/j.matpr.2021.07.310
[28] Patil S, Somasekharaiah HM, Sudarsana Rao H, Vaishali G. Effect of fly ash, silica fume, glass fiber, and polypropylene fiber on strength properties of composite fiber reinforced high-performance concrete. Int J Eng Trends Technol. 2021;69(5):69-84. https://doi.org/10.14445/22315381/IJETT-V69I5P212
[29] Afzali-Naniz O, Mazloom M. Assessment of the influence of micro- and nano-silica on the behavior of self-compacting lightweight concrete using full factorial design. Asian J Civil Eng. 2019;20:57-70. https://doi.org/10.1007/s42107-018-0088-2
[30] Chen L, Wang Z, Khan AA, Khan M, Javed MF, Alaskar A, Eldin SM. Development of predictive models for sustainable concrete via genetic programming-based algorithms. J Mater Res Technol. 2023;24:6391-410. https://doi.org/10.1016/j.jmrt.2023.04.180
[31] Abdul-Jabbar H, Khan M, Awan HH, Eldin SM, Alyousef R, Mohamed AM. Predicting ultra-high-performance concrete compressive strength using gene expression programming method. Case Stud Constr Mater. 2023;18:e02074. https://doi.org/10.1016/j.cscm.2023.e02074
[32] Islam N, Kashem A, Das P, Ali MN, Paul S. Prediction of high-performance concrete compressive strength using deep learning techniques. Asian J Civil Eng. 2023;1:1. https://doi.org/10.1007/s42107-023-00778-z
[33] Albostami AS, Al-Hamd RKS, Alzabeebee S, Minto A, Keawsawasvong S. Application of soft computing in predicting the compressive strength of self-compacted concrete containing recyclable aggregate. Asian J Civil Eng. 2024;25(1):183-96. https://doi.org/10.1007/s42107-023-00767-2
[34] Shahani NM, Ullah B, Shah KS, Hassan FU, Ali R, Elkotb MA, et al. Predicting angle of internal friction and cohesion of rocks based on machine learning algorithms. Mathematics. 2022;10(20):3875. https://doi.org/10.3390/math10203875
[35] Zada U, Jamal A, Iqbal M, Eldin SM, Almoshaogeh M, Bekkouche SR, Almuaythir S. Recent advances in expansive soil stabilization using admixtures: current challenges and opportunities. Case Stud Constr Mater. 2023;18:e01985. https://doi.org/10.1016/j.cscm.2023.e01985
[36] Caglar N, Pala M, Elmas M, Eryılmaz DM. A new approach to determine the base shear of steel frame structures. J Constr Steel Res. 2009;65(1):188-95. https://doi.org/10.1016/j.jcsr.2008.07.012
[37] Solhmirzaei R, Salehi H, Kodur V, Naser MZ. Machine learning framework for predicting failure mode and shear capacity of ultra-high-performance concrete beams. Eng Struct. 2020;224:111221. https://doi.org/10.1016/j.engstruct.2020.111221
[38] Behnood A, Golafshani EM. Machine learning study of the mechanical properties of concretes containing waste foundry sand. Constr Build Mater. 2020;243:118152. https://doi.org/10.1016/j.conbuildmat.2020.118152

[39] Shang M, Li H, Ahmad A, Ahmad W, Ostrowski KA, Aslam F, et al. Predicting the mechanical properties of RCA-based concrete using supervised machine learning algorithms. Constr Build Mater. 2022;647:1-13. https://doi.org/10.3390/ma15020647
[40] Ni HG, Wang JZ. Prediction of compressive strength of concrete by neural networks. Cem Concr Res. 2000;30(8):1245-50. https://doi.org/10.1016/S0008-8846(00)00345-8
[41] Sarıdemir M. Predicting the compressive strength of mortars containing metakaolin by artificial neural networks and fuzzy logic. Adv Eng Softw. 2009;40(9):920-7. https://doi.org/10.1016/j.advengsoft.2008.12.008
[42] Sobhani J, Najimi M, Pourkhorshidi AR, Parhizkar T. Prediction of the compressive strength of no-slump concrete: A comparative study of regression, neural network, and ANFIS models. Constr Build Mater. 2010;24(5):709-18. https://doi.org/10.1016/j.conbuildmat.2009.10.037
[43] Hodhod OA, Ahmed HI. Modeling the corrosion initiation time of slag concrete using the artificial neural network. HBRC J. 2014;10(3):231-4. https://doi.org/10.1016/j.hbrcj.2013.12.002
[44] Awoyera PO, Kirgiz MS, Viloria A, Ovallos-Gazabon D. Estimating strength properties of geopolymer self-compacting concrete using machine learning techniques. J Mater Res Technol. 2020;9(4):9016-28. https://doi.org/10.1016/j.jmrt.2020.06.008
[45] Deifalla AF, Zapris AG, Chalioris CE. Multivariable regression strength model for steel fiber-reinforced concrete beams under torsion. Materials. 2021;14(14):3889. https://doi.org/10.3390/ma14143889
[46] Nafees A, Khan S, Javed MF, Alrowais R, Mohamed AM, Mohamed A, et al. Forecasting the mechanical properties of plastic concrete employing experimental data using machine learning algorithms DT, MLPNN, SVM, and RF. Polymers. 2022;14(8):1583. https://doi.org/10.3390/polym14081583
[47] Salem NM, Deifalla A. Evaluation of the strength of slab-column connections with FRPs using machine learning algorithms. Polymers. 2022;14(8):1517. https://doi.org/10.3390/polym14081517
[48] Azam R, Riaz MR, Farooq MU, Ali F, Mohsan M, Deifalla AF, et al. Optimization-based economical flexural design of singly reinforced concrete beams: a parametric study. Materials. 2022;15(9):3223. https://doi.org/10.3390/ma15093223
[49] Li Y, Zhang Q, Kamiński P, Deifalla AF, Sufian M, Dyczko A, et al. Compressive strength of steel fiber-reinforced concrete employing supervised machine learning techniques. Materials. 2022;15(12):4209. https://doi.org/10.3390/ma15124209
[50] Nafees A, Javed MF, Khan S, Nazir K, Farooq F, Aslam F, et al. Predictive modeling of mechanical properties of silica fume-based green concrete using artificial intelligence approaches: MLPNN, ANFIS, and GEP. Materials. 2021;14(24):7531. https://doi.org/10.3390/ma14247531
[51] Khan M, Lao J, Dai JG. Comparative study of advanced computational techniques for estimating the compressive strength of UHPC. J Asian Concr Fed. 2022;8(1):51-68. https://doi.org/10.18702/acf.2022.6.8.1.51
[52] Anwar MK, Shah SAR, Azab M, Shah I, Chauhan MKS, Iqbal F. Structural performance of GFRP bars based high-strength RC columns: an application of advanced decision-making mechanism for experimental profile data. Buildings. 2022;12(5):611. https://doi.org/10.3390/buildings12050611
[53] Shah SAR, Azab M, Seif ElDin HM, Barakat O, Anwar MK, Bashir Y. Predicting compressive strength of blast furnace slag and fly ash-based sustainable concrete using machine learning techniques: an application of advanced decision-making approaches. Buildings. 2022;12(7):914. https://doi.org/10.3390/buildings12070914
[54] Hulipalled P, Algur V, Lokesha V. An approach of data science for the prediction of wear behaviour of hypereutectoid steel. J Bio Tribo-Corros. 2022;8(3):69. https://doi.org/10.1007/s40735-022-00668-y
[55] Hulipalled P, Algur V, Lokesha V, Saumya S. Interpretable ensemble machine learning framework to predict wear rate of modified ZA-27 alloy. Tribol Int. 2023;188:108783. https://doi.org/10.1016/j.triboint.2023.108783
[56] Hulipalled P, Algur V, Lokesha V, Saumya S. Intelligent retrieval of wear rate prediction for hypereutectoid steel. Multiscale Multidiscip Model Exp Des. 2023;6(4):629-41. https://doi.org/10.1007/s41939-023-00172-x
[57] Hulipalled P, Lokesha V. Optimized machine learning algorithms to predict wear behavior of tribo-informatics. 2022. https://doi.org/10.21203/rs.3.rs-2159217/v1
[58] Hulipalled P, Lokesha V. Intelligent prediction of wear loss based on ensemble learning in dual-phase steel. J Int Acad Phys Sci. 2023;27(2):161-70.
[59] Carmichael RP. Relationships between young's modulus, compressive strength, poisson's ratio, and time for early age concrete. Swarthmore College. 2009.
[60] Bal L, Buyle-Bodin F. Artificial neural network for predicting drying shrinkage of concrete. Constr Build Mater. 2013;38:248-54. https://doi.org/10.1016/j.conbuildmat.2012.08.043